Stable high order methods for time-domain wave propagation in complex geometries and heterogeneous media

Jesse Chan

Department of Computational and Applied Mathematics, Rice University

University of Houston
Electromagnetics seminar
April 10, 2020

Collaborators in wave propagation

Tim Warburton (Virginia Tech)

Russell Hewett (Virginia Tech)

Sebastian Acosta (BCM, TCH)

Kaihang Guo (Rice, PhD 2021)

Numerical simulation of wave propagation

Many procedures require **accurately** and **efficiently** simulating solving time-dependent wave equations in realistic settings.

- Imaging (seismic, medical)
- Engineering design (scattering, design)
- Computational physics (aeroacoustics, astrophysics)

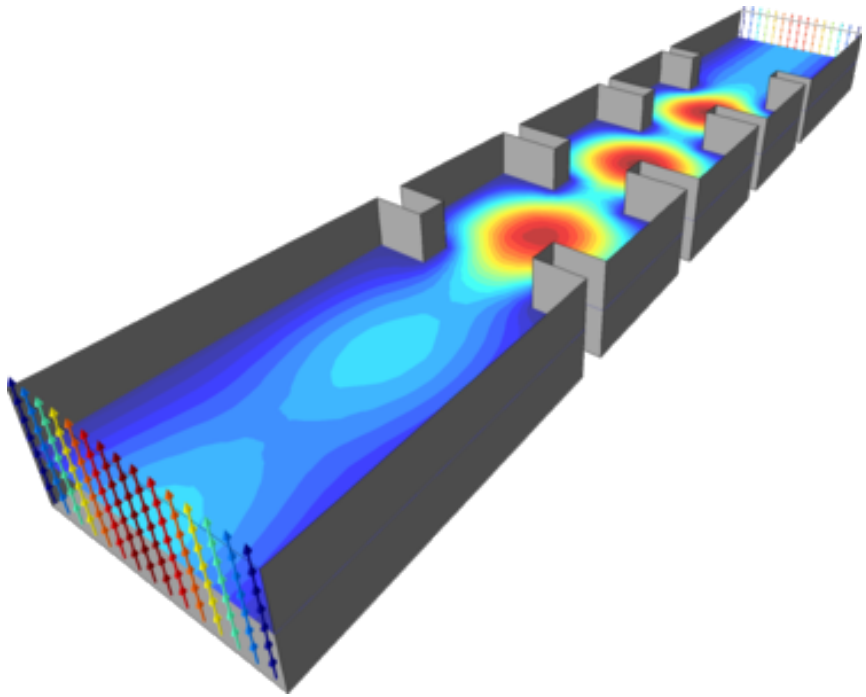

https://www.comsol.com/model/image/12737/big.png

Discontinuous Galerkin (DG) methods for waves

- Unstructured (tetrahedral) meshes for geometric flexibility.
- High order: low numerical dissipation and dispersion.
- High order approximations: more accurate per unknown.
- Explicit time stepping: high performance on many-core.

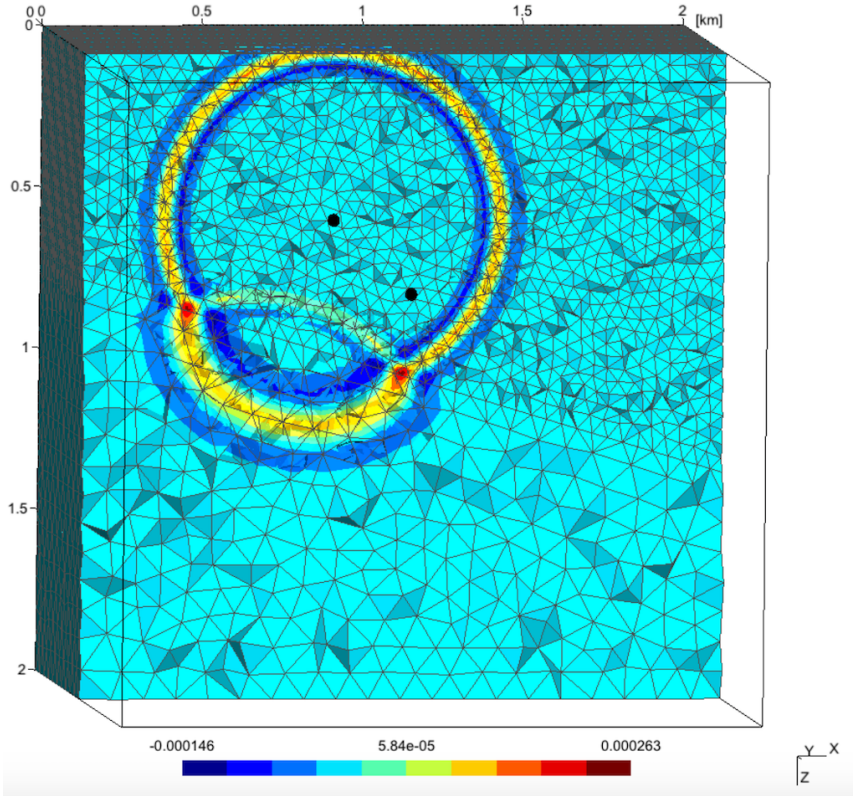

Figure courtesy of Axel Modave.

Goal: stability **and** efficiency for heterogeneous media.

Discontinuous Galerkin (DG) methods for waves

- Unstructured (tetrahedral) meshes for geometric flexibility.
- High order: low numerical dissipation and dispersion.
- High order approximations: more accurate per unknown.
- Explicit time stepping: high performance on many-core.

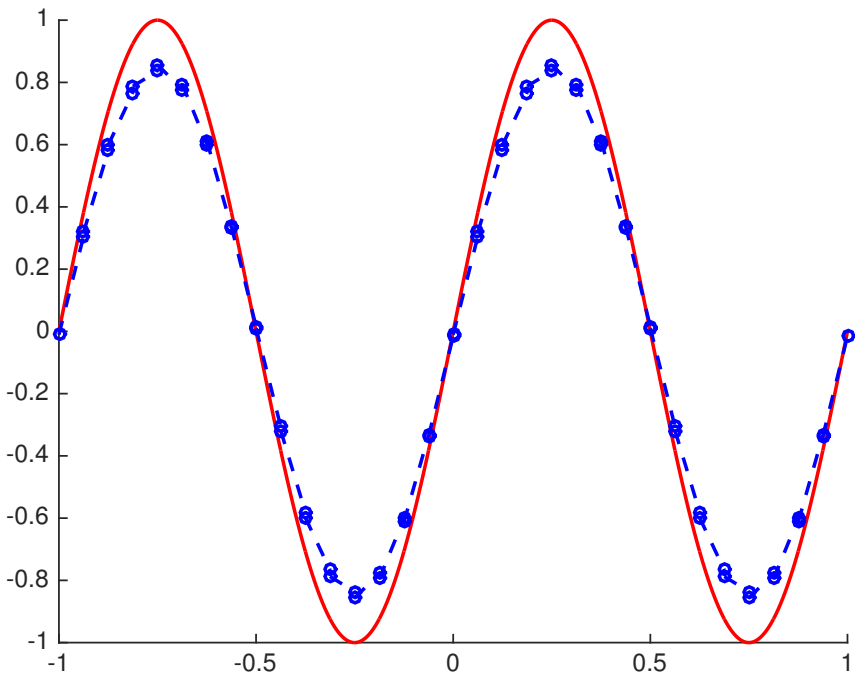

Fine linear approximation.

Goal: stability **and** efficiency for heterogeneous media.

Discontinuous Galerkin (DG) methods for waves

- Unstructured (tetrahedral) meshes for geometric flexibility.
- High order: low numerical dissipation and dispersion.
- High order approximations: more accurate per unknown.
- Explicit time stepping: high performance on many-core.

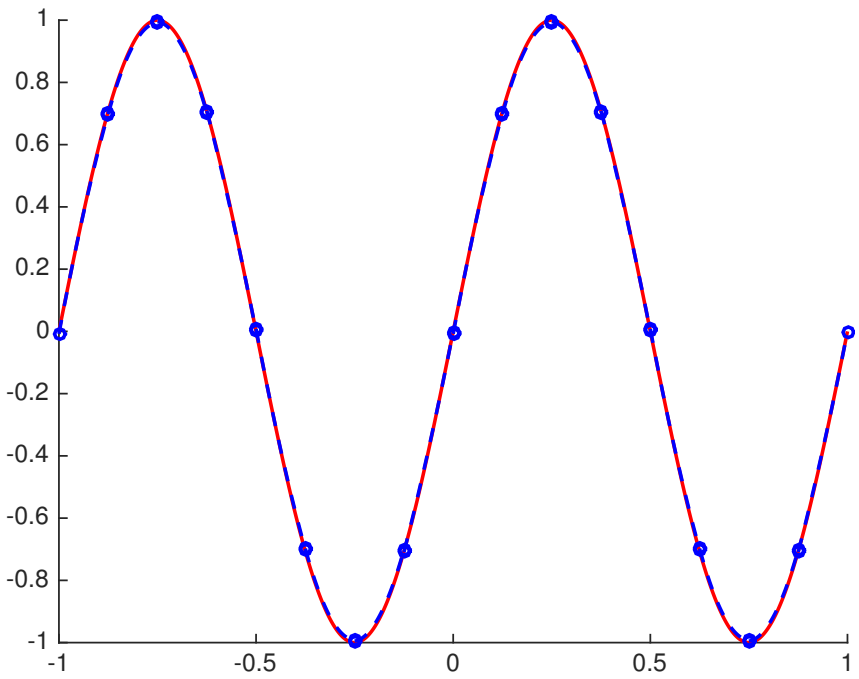

Coarse quadratic approximation.

Goal: stability **and** efficiency for heterogeneous media.

Discontinuous Galerkin (DG) methods for waves

- Unstructured (tetrahedral) meshes for geometric flexibility.
- High order: low numerical dissipation and dispersion.
- High order approximations: more accurate per unknown.
- Explicit time stepping: high performance on many-core.

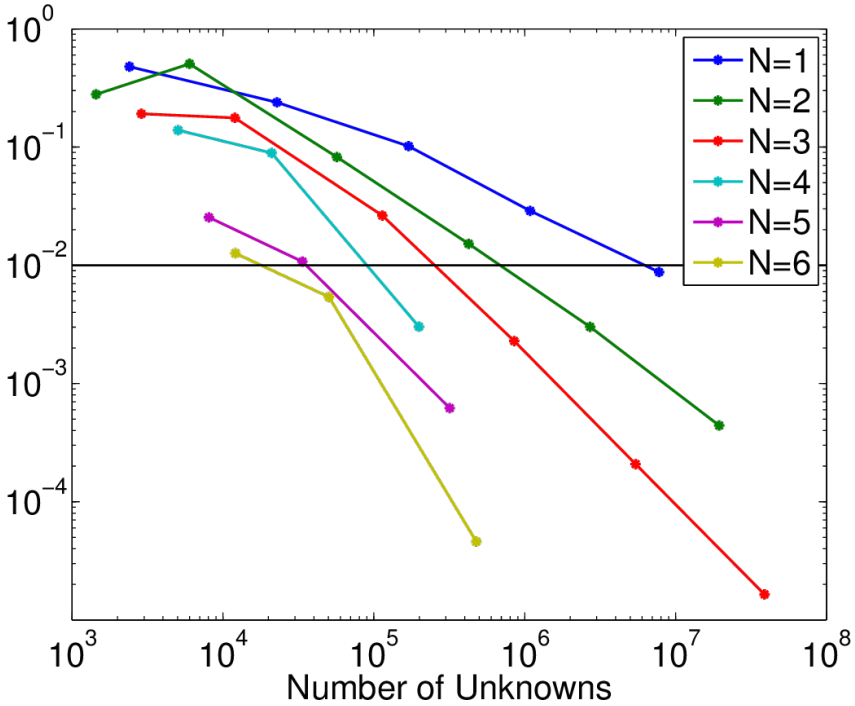

Max errors vs. dofs.

Goal: stability **and** efficiency for heterogeneous media.

Discontinuous Galerkin (DG) methods for waves

- Unstructured (tetrahedral) meshes for geometric flexibility.
- High order: low numerical dissipation and dispersion.
- High order approximations: more accurate per unknown.
- Explicit time stepping: high performance on many-core.

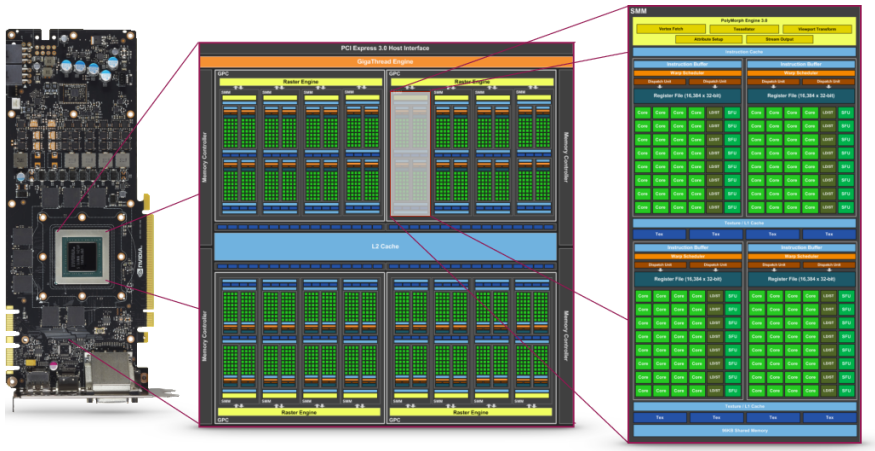

Graphics processing units (GPU).

Goal: stability **and** efficiency for heterogeneous media.

Discontinuous Galerkin (DG) methods for waves

- Unstructured (tetrahedral) meshes for geometric flexibility.
- High order: low numerical dissipation and dispersion.
- High order approximations: more accurate per unknown.
- Explicit time stepping: high performance on many-core.

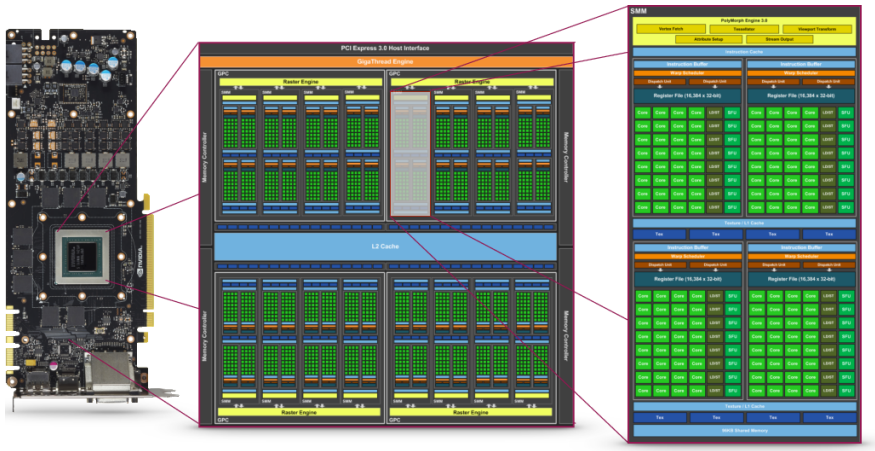

Graphics processing units (GPU).

Goal: stability **and** efficiency for heterogeneous media.

High order nodal discontinuous Galerkin methods

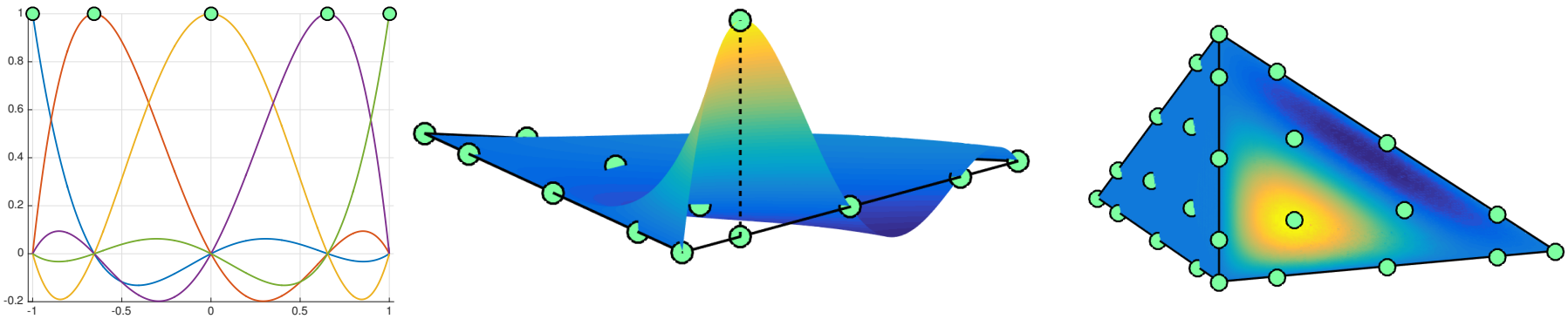

Lagrange (nodal) bases on a line, triangle, tetrahedron.

- Nodal bases defined implicitly through an orthogonal basis.
- Point locations optimized for interpolation and numerical stability.
- Assume **affine** tetrahedra, coefficients **constant** on each element.

Time-domain nodal DG methods

Assume $u(\boldsymbol{x}, t) = \sum \boldsymbol{u}_j \phi_j(\boldsymbol{x})$ on D^k

- Compute numerical flux at face nodes (non-local).
- Compute RHS of (local) ODE.
- Evolve (local) solution using explicit time integration (RK, AB, etc).

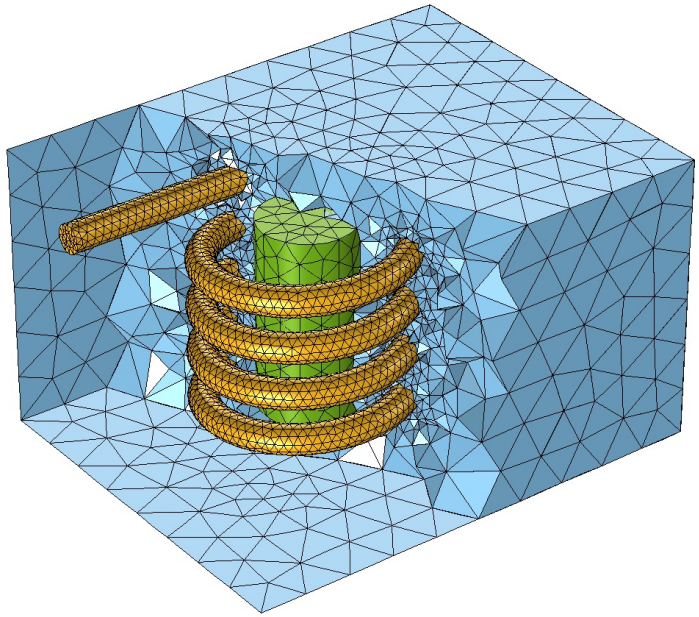

Mesh from COMSOL

$$\frac{\partial u}{\partial t} = \frac{\partial u}{\partial x}$$

Example: advection equation.

$$\boldsymbol{M}_{ij} = \int_{D^k} \phi_j(\boldsymbol{x}) \phi_i(\boldsymbol{x})$$

$$\mathbf{L}_f = \mathbf{M}^{-1} \mathbf{M}_f.$$

Time-domain nodal DG methods

Assume $u(\boldsymbol{x}, t) = \sum \boldsymbol{u}_j \phi_j(\boldsymbol{x})$ on D^k

- Compute numerical flux at face nodes (non-local).
- Compute RHS of (local) ODE.
- Evolve (local) solution using explicit time integration (RK, AB, etc).

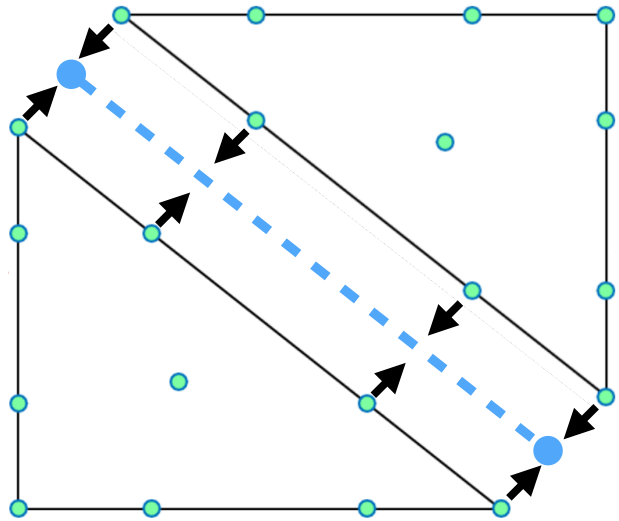

$$\frac{\mathrm{d}\mathbf{u}}{\mathrm{d}t} = \mathbf{D}_x \mathbf{u} + \sum_{\text{faces}} \mathbf{L}_f \left(\text{flux}\right).$$

$$\boldsymbol{M}_{ij} = \int_{D^k} \phi_j(\boldsymbol{x}) \phi_i(\boldsymbol{x})$$

$$\mathbf{L}_f = \mathbf{M}^{-1} \mathbf{M}_f.$$

Time-domain nodal DG methods

Assume $u(\boldsymbol{x}, t) = \sum \boldsymbol{u}_j \phi_j(\boldsymbol{x})$ on D^k

- Compute numerical flux at face nodes (non-local).
- Compute RHS of (local) ODE.
- Evolve (local) solution using explicit time integration (RK, AB, etc).

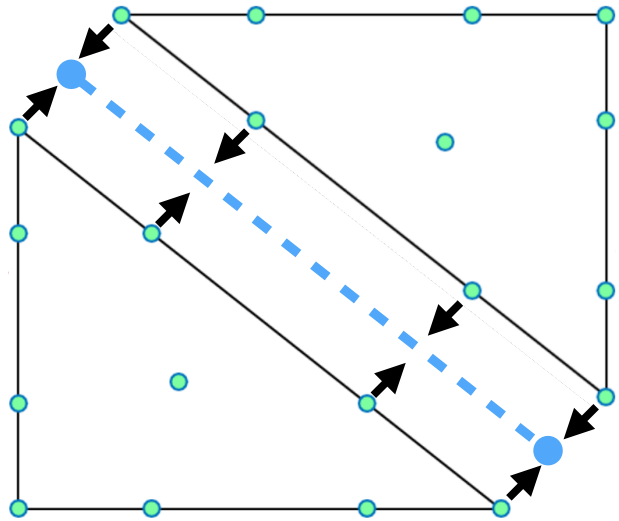

$$\frac{\mathrm{d}\mathbf{u}}{\mathrm{d}t} = \underbrace{\mathbf{D}_x \mathbf{u}}_{\text{Volume kernel}} + \underbrace{\sum_{\text{faces}} \mathbf{L}_f \, (\text{flux})}_{\text{Surface kernel}}.$$

$$\boldsymbol{M}_{ij} = \int_{D^k} \phi_j(\boldsymbol{x}) \phi_i(\boldsymbol{x})$$

$$\mathbf{L}_f = \mathbf{M}^{-1} \mathbf{M}_f.$$

Time-domain nodal DG methods

Assume $u(\boldsymbol{x}, t) = \sum \boldsymbol{u}_j \phi_j(\boldsymbol{x})$ on D^k

- Compute numerical flux at face nodes (non-local).
- Compute RHS of (local) ODE.
- Evolve (local) solution using explicit time integration (RK, AB, etc).

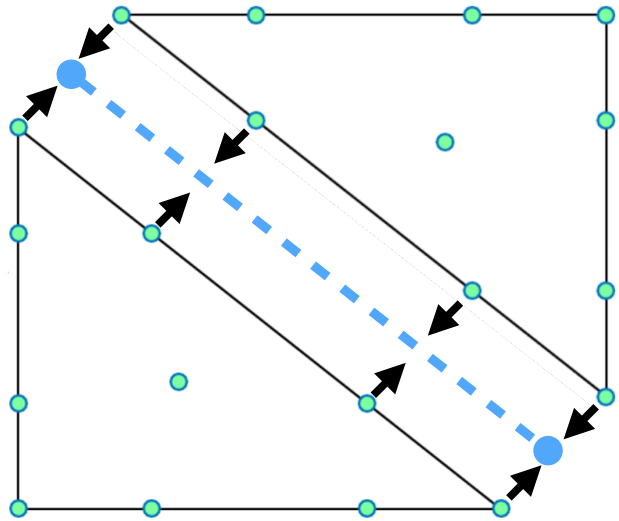

$$\underbrace{\frac{\mathrm{d}\mathbf{u}}{\mathrm{d}t}}_{\text{Update kernel}} = \underbrace{\mathbf{D}_x \mathbf{u}}_{\text{Volume kernel}} + \underbrace{\sum_{\text{faces}} \mathbf{L}_f \left(\text{flux}\right)}_{\text{Surface kernel}}.$$

$$\boldsymbol{M}_{ij} = \int_{D^k} \phi_j(\boldsymbol{x}) \phi_i(\boldsymbol{x})$$

$$\mathbf{L}_f = \mathbf{M}^{-1} \mathbf{M}_f.$$

Outline

1. Weight-adjusted DG (WADG) methods
   - High order heterogeneous media
   - Curvilinear meshes
2. Elastic and coupled acoustic-elastic media
3. Bernstein-Bezier WADG: high order efficiency

Outline

1 Weight-adjusted DG (WADG) methods
- High order heterogeneous media
- Curvilinear meshes

2 Elastic and coupled acoustic-elastic media

3 Bernstein-Bezier WADG: high order efficiency

Energy stable discontinuous Galerkin formulations

- Model problem: acoustic wave equation

$$\frac{1}{c^2}\frac{\partial p}{\partial t} = \nabla \cdot \boldsymbol{u}, \qquad \frac{\partial \boldsymbol{u}}{\partial t} = \nabla p$$

- (Local) formulation with simple penalty fluxes

$$\int_{D^k} \frac{1}{c^2}\frac{\partial p}{\partial t} q = \int_{D^k} \nabla \cdot \boldsymbol{u} q + \frac{1}{2}\int_{\partial D^k} \left([\![\boldsymbol{u}]\!] \cdot \boldsymbol{n} + \tau_p [\![p]\!] \right) q$$

$$\int_{D^k} \frac{\partial \boldsymbol{u}}{\partial t} \boldsymbol{v} = \int_{D^k} \nabla p \cdot \boldsymbol{v} + \frac{1}{2}\int_{\partial D^k} \left([\![p]\!] + \tau_u [\![\boldsymbol{u}]\!] \cdot \boldsymbol{n} \right) \boldsymbol{v}$$

- High order accuracy, semi-discrete energy stability

$$\frac{\partial}{\partial t}\left(\sum_k \int_{D^k} \frac{p^2}{c^2} + |\boldsymbol{u}|^2 \right) = -\sum_k \int_{\partial D^k} \tau_p [\![p]\!]^2 + \tau_u \left([\![\boldsymbol{u}]\!] \cdot \boldsymbol{n} \right)^2 \leq 0.$$

High order approximation of media and geometry

- Efficient implementation on **simplicial** meshes: c^2 piecewise constant, non-curved meshes (J, J^f piecewise constant).

$$\int_{D^k} \frac{1}{c^2}\frac{\partial p}{\partial t} q = \int_{D^k} \nabla \cdot \boldsymbol{u} q + \frac{1}{2}\int_{\partial D^k} (\llbracket \boldsymbol{u} \rrbracket \cdot \boldsymbol{n} + \tau_p \llbracket p \rrbracket)\, q$$

$$\int_{D^k} \frac{\partial \boldsymbol{u}}{\partial t} \boldsymbol{v} = \int_{D^k} \nabla p \cdot \boldsymbol{v} + \frac{1}{2}\int_{\partial D^k} (\llbracket p \rrbracket + \tau_u \llbracket \boldsymbol{u} \rrbracket \cdot \boldsymbol{n})\, \boldsymbol{v}$$

- Spurious reflections for low order approximations of media, geometry.

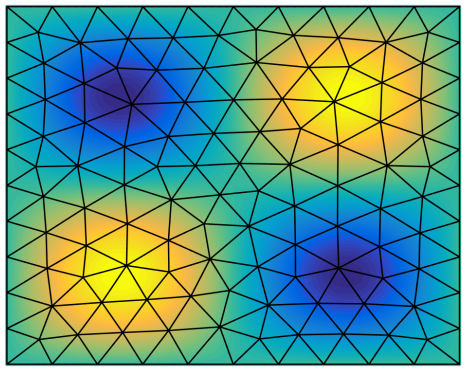

(a) Mesh and exact c^2

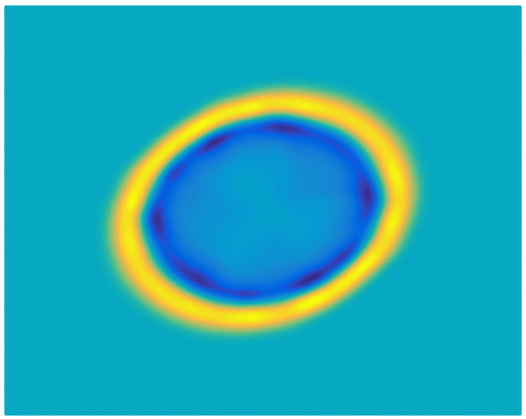

(b) Piecewise const. c^2

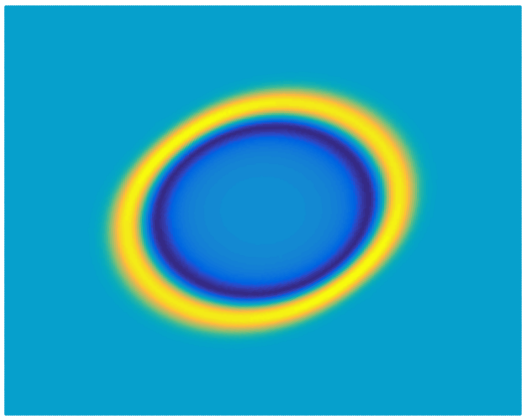

(c) High order c^2

High order approximation of media and geometry

- Efficient implementation on **simplicial** meshes: c^2 piecewise constant, non-curved meshes (J, J^f piecewise constant).

$$\int_{\widehat{D}} \frac{1}{c^2} \frac{\partial p}{\partial t} q J = \int_{\widehat{D}} \nabla \cdot \boldsymbol{u} q J + \frac{1}{2} \int_{\partial \widehat{D}} \left([\![\boldsymbol{u}]\!] \cdot \boldsymbol{n} + \tau_p [\![p]\!] \right) q J^f$$

$$\int_{\widehat{D}} \frac{\partial \boldsymbol{u}}{\partial t} \boldsymbol{v} J = \int_{\widehat{D}} \nabla p \cdot \boldsymbol{v} J + \frac{1}{2} \int_{\partial \widehat{D}} \left([\![p]\!] + \tau_u [\![\boldsymbol{u}]\!] \cdot \boldsymbol{n} \right) \boldsymbol{v} J^f$$

- Spurious reflections for low order approximations of media, geometry.

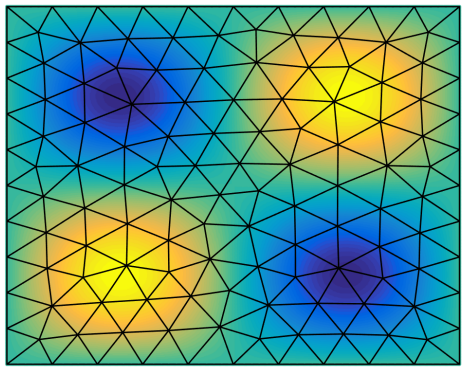

(a) Mesh and exact c^2

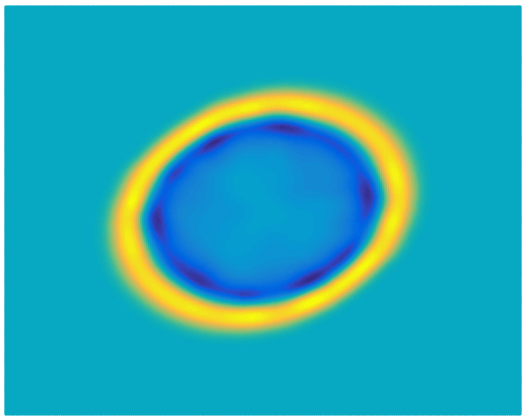

(b) Piecewise const. c^2

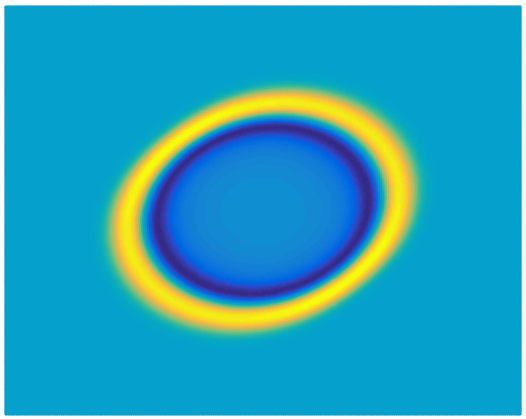

(c) High order c^2

High order approximation of media and geometry

- Efficient implementation on **simplicial** meshes: c^2 piecewise constant, non-curved meshes (J, J^f piecewise constant).

$$\frac{J}{c^2}\int_{\widehat{D}}\frac{\partial p}{\partial t}q = J\int_{\widehat{D}}\nabla\cdot\boldsymbol{u}q + J^f\frac{1}{2}\int_{\partial\widehat{D}}\left(\llbracket\boldsymbol{u}\rrbracket\cdot\boldsymbol{n}+\tau_p\llbracket p\rrbracket\right)q$$

$$J\int_{\widehat{D}}\frac{\partial \boldsymbol{u}}{\partial t}\boldsymbol{v} = J\int_{\widehat{D}}\nabla p\cdot\boldsymbol{v} + J^f\frac{1}{2}\int_{\partial\widehat{D}}\left(\llbracket p\rrbracket+\tau_u\llbracket\boldsymbol{u}\rrbracket\cdot\boldsymbol{n}\right)\boldsymbol{v}$$

- Spurious reflections for low order approximations of media, geometry.

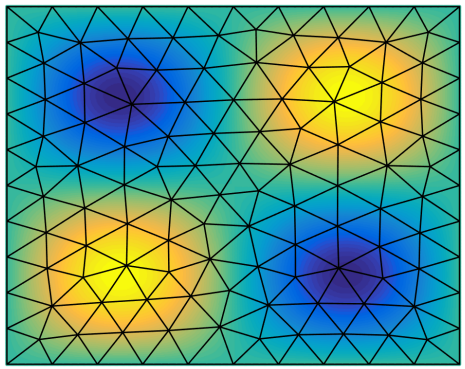

(a) Mesh and exact c^2

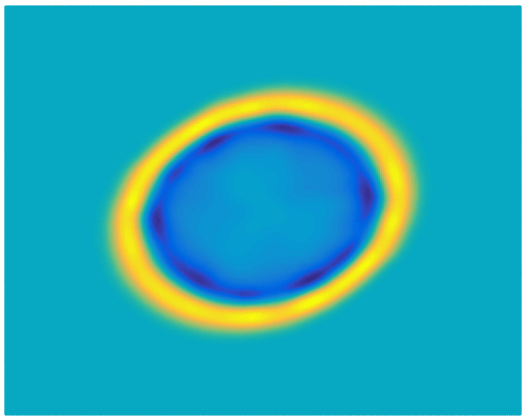

(b) Piecewise const. c^2

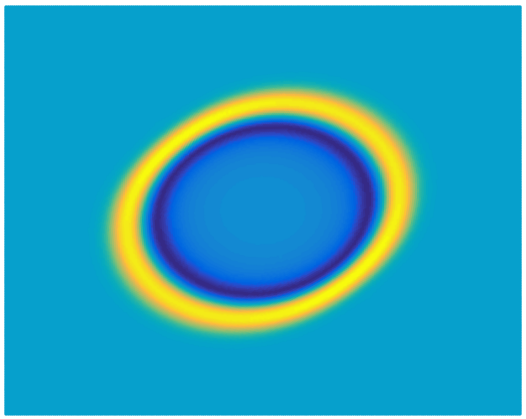

(c) High order c^2

Weighted mass matrices

- Spatially varying weights appear in DG mass matrices

$$\int_{\widehat{D}} \frac{1}{c^2} \frac{\partial p}{\partial t} q J = \text{pressure RHS}, \qquad \int_{\widehat{D}} \frac{\partial \boldsymbol{u}}{\partial t} \boldsymbol{v} J = \text{velocity RHS}$$

- Curvilinear meshes and wave propagation in heterogeneous media

$$(\boldsymbol{M}_w)_{ij} = \int_{\widehat{D}} \phi_i \phi_j w(x),$$

$$\frac{\mathrm{d}}{\mathrm{d}t} \boldsymbol{M}_w \boldsymbol{u} = \text{right hand side}.$$

- Inherits **high order accuracy** and **energy stability** with respect to a weighted L^2 norm, but requires $\boldsymbol{M}_w^{-1}$ explicitly over each element.

Weighted mass matrices

- Spatially varying weights appear in DG mass matrices

$$\int_{\widehat{D}} \frac{1}{c^2} \frac{\partial p}{\partial t} q J = \text{pressure RHS}, \qquad \int_{\widehat{D}} \frac{\partial \boldsymbol{u}}{\partial t} \boldsymbol{v} J = \text{velocity RHS}$$

- Curvilinear meshes and wave propagation in heterogeneous media

$$(\boldsymbol{M}_w)_{ij} = \int_{\widehat{D}} \phi_i \phi_j J(x),$$

$$\frac{\mathrm{d}}{\mathrm{d}t} \boldsymbol{M}_J \boldsymbol{u} = \text{right hand side}.$$

- Inherits **high order accuracy** and **energy stability** with respect to a weighted L^2 norm, but requires $\boldsymbol{M}_w^{-1}$ explicitly over each element.

Weighted mass matrices

- Spatially varying weights appear in DG mass matrices

$$\int_{\widehat{D}} \frac{1}{c^2} \frac{\partial p}{\partial t} q J = \text{pressure RHS}, \qquad \int_{\widehat{D}} \frac{\partial \boldsymbol{u}}{\partial t} \boldsymbol{v} J = \text{velocity RHS}$$

- Curvilinear meshes and wave propagation in heterogeneous media

$$(\boldsymbol{M}_w)_{ij} = \int_{\widehat{D}} \phi_i \phi_j \frac{J}{c^2(x)},$$

$$\frac{\mathrm{d}}{\mathrm{d}t} \boldsymbol{M}_{J/c^2} \boldsymbol{u} = \text{right hand side}.$$

- Inherits **high order accuracy** and **energy stability** with respect to a weighted L^2 norm, but requires $\boldsymbol{M}_w^{-1}$ explicitly over each element.

Weighted mass matrices

- Spatially varying weights appear in DG mass matrices

$$\int_{\widehat{D}} \frac{1}{c^2} \frac{\partial p}{\partial t} q J = \text{pressure RHS}, \qquad \int_{\widehat{D}} \frac{\partial \boldsymbol{u}}{\partial t} \boldsymbol{v} J = \text{velocity RHS}$$

- Curvilinear meshes and wave propagation in heterogeneous media

$$(\boldsymbol{M}_w)_{ij} = \int_{\widehat{D}} \phi_i \phi_j w(x),$$

$$\frac{\mathrm{d}}{\mathrm{d}t} \boldsymbol{M}_w \boldsymbol{u} = \text{right hand side}.$$

- Inherits **high order accuracy** and **energy stability** with respect to a weighted L^2 norm, but requires $\boldsymbol{M}_w^{-1}$ explicitly over each element.

Inverting weighted mass matrices: storage costs

- Assembling and inverting $\boldsymbol{M}_w$ on-the-fly
  - High computational complexity w.r.t. N.
  - Fine-grain parallelization of solve more difficult.
- Pre-computation and storage of $\boldsymbol{M}_w^{-1}$
  - Increase from $O(N^3)$ to $O(N^6)$ storage per element.

Memory costs of DG (*single precision*, one field, 3D tets, 1M elements):

Order N	$N = 1$	$N = 3$	$N = 5$	$N = 7$
Block matrix M^{-1}	.298 GB	3.2 GB	25.08 GB	115.2 GB
Solution dofs	.075 GB	.16 GB	.448 GB	.96 GB

Weight-adjusted DG (WADG)

- Weight-adjusted DG: provably energy stable approx. of $\boldsymbol{M}_{1/c^2}$

$$\boldsymbol{M}_w \frac{\mathrm{d}\boldsymbol{p}}{\mathrm{d}t} \approx \boldsymbol{M} \left(\boldsymbol{M}_{1/w}\right)^{-1} \boldsymbol{M} \frac{\mathrm{d}\boldsymbol{p}}{\mathrm{d}t} = \boldsymbol{A}_h \boldsymbol{U}.$$

- New evaluation reuses non-weighted implementation

$$\frac{\mathrm{d}\boldsymbol{p}}{\mathrm{d}t} = \underbrace{\boldsymbol{M}^{-1}\left(\boldsymbol{M}_{1/w}\right)}_{\text{modified update}} \qquad \underbrace{\boldsymbol{M}^{-1}\boldsymbol{A}_h\boldsymbol{U}}_{\text{constant wavespeed RHS}}$$

- Low-storage: form $\boldsymbol{M}_{1/w}$ on-the-fly using quadrature.

Chan, Hewett, Warburton (2017). Weight-adjusted DG methods: wave propagation in heterogeneous media.

Highlights of WADG theory

- WADG norm has same equivalence constants (doesn't hurt CFL)

$$w_{\min} \boldsymbol{u}^T \boldsymbol{M} \boldsymbol{u} \leq \boldsymbol{u}^T \boldsymbol{M}_w \boldsymbol{u} \leq w_{\max} \boldsymbol{u}^T \boldsymbol{M} \boldsymbol{u}$$

- High order accurate approx. to full inverse weighted mass matrix, local conservation if weight $w(\boldsymbol{x})$ approximated using polynomials.

- Best L^2 approximation error is $O(h^{N+1})$, while difference between full inverse weighted mass matrix and WADG is $O\left(h^{N+2}\right)$

$$\left\| P_w u - \widetilde{P}_w u \right\|_{L^2} \leq C_{w,N} h^{N+2} \left\| w \right\|_{W^{N+1,\infty}} \left\| u \right\|_{W^{N+1,2}}$$

Chan, Hewett, Warburton (2017). Weight-adjusted DG methods: wave propagation in heterogeneous media.

Highlights of WADG theory

- WADG norm has same equivalence constants (doesn't hurt CFL)

$$w_{\min} \boldsymbol{u}^T \boldsymbol{M} \boldsymbol{u} \leq \boldsymbol{u}^T \boldsymbol{M} \boldsymbol{M}_{1/w}^{-1} \boldsymbol{M} \boldsymbol{u} \leq w_{\max} \boldsymbol{u}^T \boldsymbol{M} \boldsymbol{u}$$

- High order accurate approx. to full inverse weighted mass matrix, local conservation if weight $w(\boldsymbol{x})$ approximated using polynomials.

- Best L^2 approximation error is $O(h^{N+1})$, while difference between full inverse weighted mass matrix and WADG is $O\left(h^{N+2}\right)$

$$\left\| P_w u - \widetilde{P}_w u \right\|_{L^2} \leq C_{w,N} h^{N+2} \left\| w \right\|_{W^{N+1,\infty}} \left\| u \right\|_{W^{N+1,2}}$$

Chan, Hewett, Warburton (2017). Weight-adjusted DG methods: wave propagation in heterogeneous media.

WADG: nearly identical to DG w/weighted mass matrices

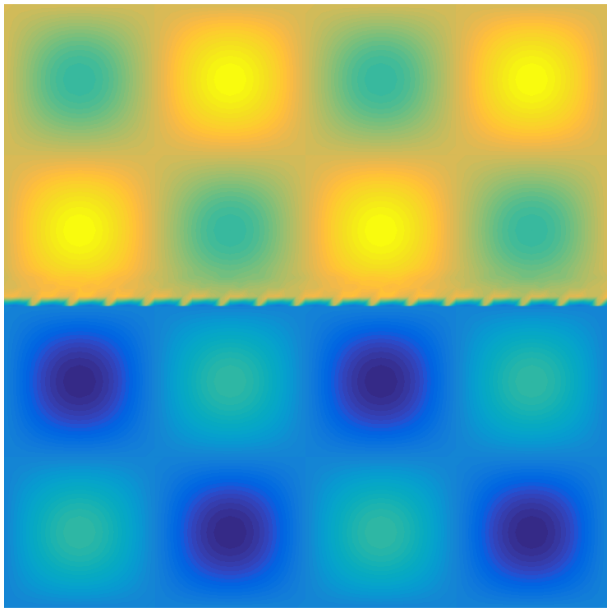

(a) $c^2(x, y)$

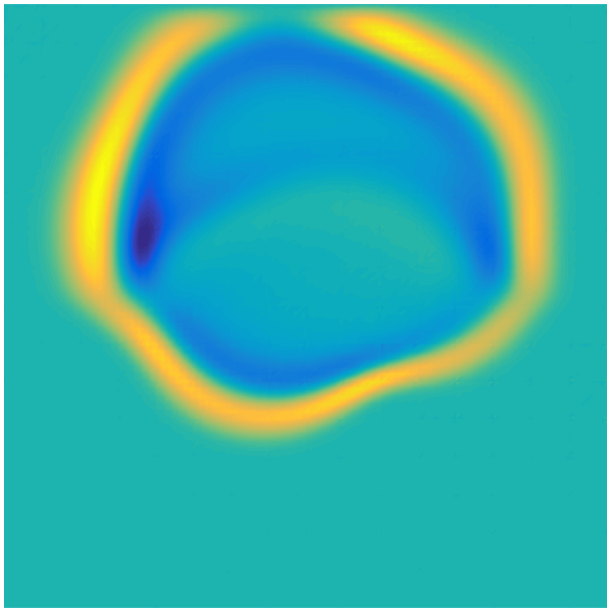

(b) Standard DG

Figure: Standard vs. weight-adjusted DG with spatially varying c^2.

- The L^2 error is $O(h^{N+1})$, but the difference between the DG and WADG solutions is $O(h^{N+2})$!

WADG: nearly identical to DG w/weighted mass matrices

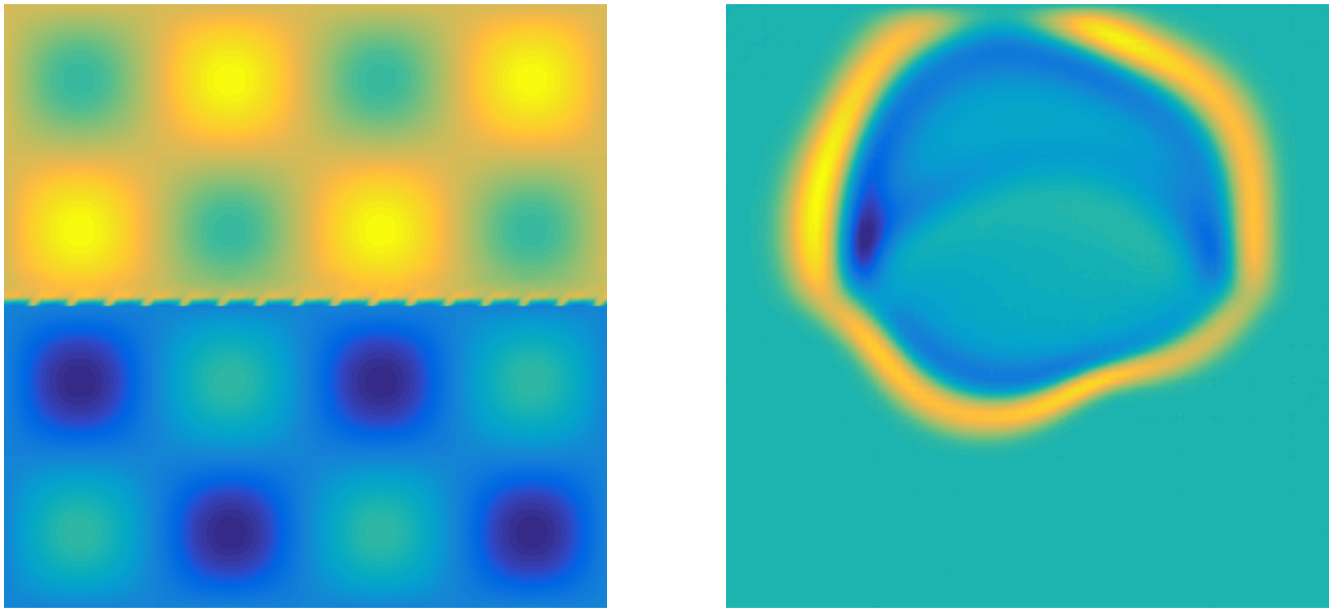

(a) $c^2(x, y)$ (b) Weighted-adjusted DG

Figure: Standard vs. weight-adjusted DG with spatially varying c^2.

- The L^2 error is $O(h^{N+1})$, but the difference between the DG and WADG solutions is $O(h^{N+2})$!

Outline

1. Weight-adjusted DG (WADG) methods
   - High order heterogeneous media
   - Curvilinear meshes
2. Elastic and coupled acoustic-elastic media
3. Bernstein-Bezier WADG: high order efficiency

Acoustics, variable coefficients: L^2 errors

Smooth wavefield $c^2(x,y) = 1 + \frac{1}{2}\sin(\pi x)\sin(\pi y)$

	$h = 1$	$h = 1/2$	$h = 1/4$	$h = 1/8$
DG $N = 1$	2.13e-01	6.25e-02	1.64e-02	4.19e-03
WADG $N = 1$	2.05e-01	5.99e-02	1.62e-02	4.18e-03
DG $N = 2$	3.01e-02	3.60e-03	4.21e-04	5.07e-05
WADG $N = 2$	2.89e-02	3.54e-03	4.18e-04	5.07e-05
DG $N = 3$	6.10e-03	3.33e-04	2.04e-05	1.22e-06
WADG $N = 3$	8.69e-03	3.47e-04	2.03e-05	1.22e-06
DG $N = 4$	6.61e-04	2.12e-05	6.39e-07	1.94e-08
WADG $N = 4$	1.09e-03	2.27e-05	6.30e-07	1.93e-08

Table: Convergence of standard, weight-adjusted DG to a manufactured solution.

Acoustics, variable coefficients: L^2 errors

Smooth wavefield $c^2(x,y) = 1 + \frac{1}{2}\sin(\pi x)\sin(\pi y)$

	$h = 1$	$h = 1/2$	$h = 1/4$	$h = 1/8$
DG $N = 1$	2.48e-01	7.58-02	1.69e-02	4.46e-03
WADG $N = 1$	2.50e-01	7.72e-02	1.69e-02	4.47e-03
DG $N = 2$	5.95e-02	9.95e-03	1.10e-03	1.22e-04
WADG $N = 2$	6.09e-02	1.02e-02	1.10e-03	1.22e-04
DG $N = 3$	2.29e-02	1.98e-03	9.52e-05	6.56e-06
WADG $N = 3$	1.98e-02	1.98e-03	9.52e-05	6.56e-06
DG $N = 4$	4.90e-03	3.01e-04	1.78e-05	7.27e-07
WADG $N = 4$	4.64e-03	3.02e-04	1.78e-05	7.28e-07

Table: Convergence to a reference solution ($N = 100$ spectral method).

WADG: more efficient than storing $\boldsymbol{M}_w^{-1}$ on GPUs

	$N=1$	$N=2$	$N=3$	$N=4$	$N=5$	$N=6$	$N=7$
$\boldsymbol{M}_{1/c^2}^{-1}$	.66	2.79	9.90	29.4	73.9	170.5	329.4
WADG	0.59	1.44	4.30	13.9	43.0	107.8	227.7
Speedup	1.11	1.94	2.30	2.16	1.72	1.58	1.45

Time (ns) per element: storing/applying $\boldsymbol{M}_w^{-1}$ vs WADG (deg. $2N$ quadrature).

- Low storage matrix-free application of $\boldsymbol{M}^{-1}\boldsymbol{M}_{1/w}$ using **quadrature**-based interpolation and L^2 projection matrices $\boldsymbol{V}_q, \boldsymbol{P}_q$.

$$(\boldsymbol{M})^{-1}\boldsymbol{M}_{1/w} = \underbrace{\boldsymbol{M}^{-1}\boldsymbol{V}_q^T\boldsymbol{W}}_{\boldsymbol{P}_q}\operatorname{diag}(1/w)\,\boldsymbol{V}_q.$$

- Low storage WADG faster than storing and applying $\boldsymbol{M}_w^{-1}$ on GPUs.

WADG: more efficient than storing M_w^{-1} on GPUs

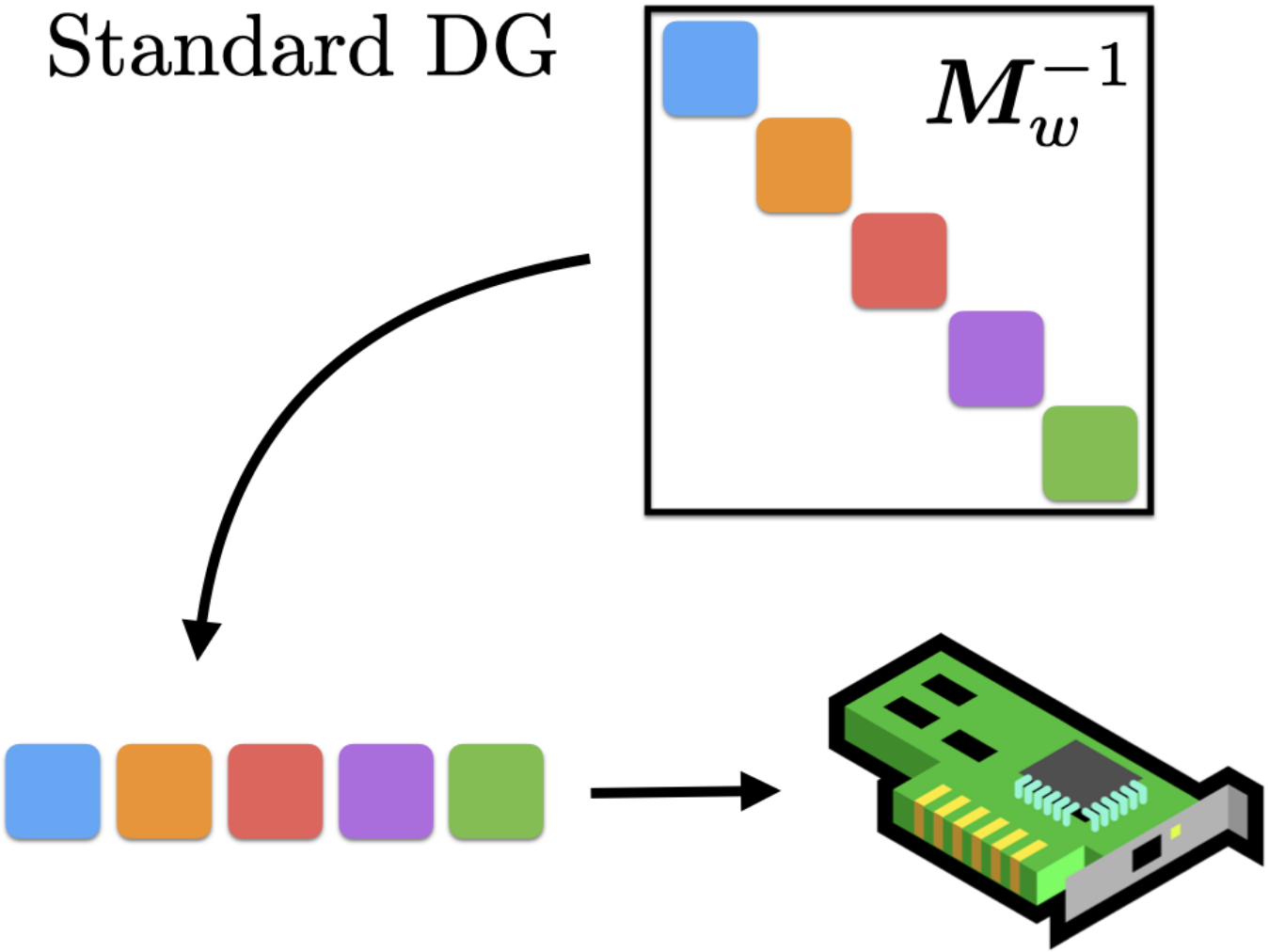

Efficiency on GPUs: reduce memory accesses and data movement!

WADG: more efficient than storing M_w^{-1} on GPUs

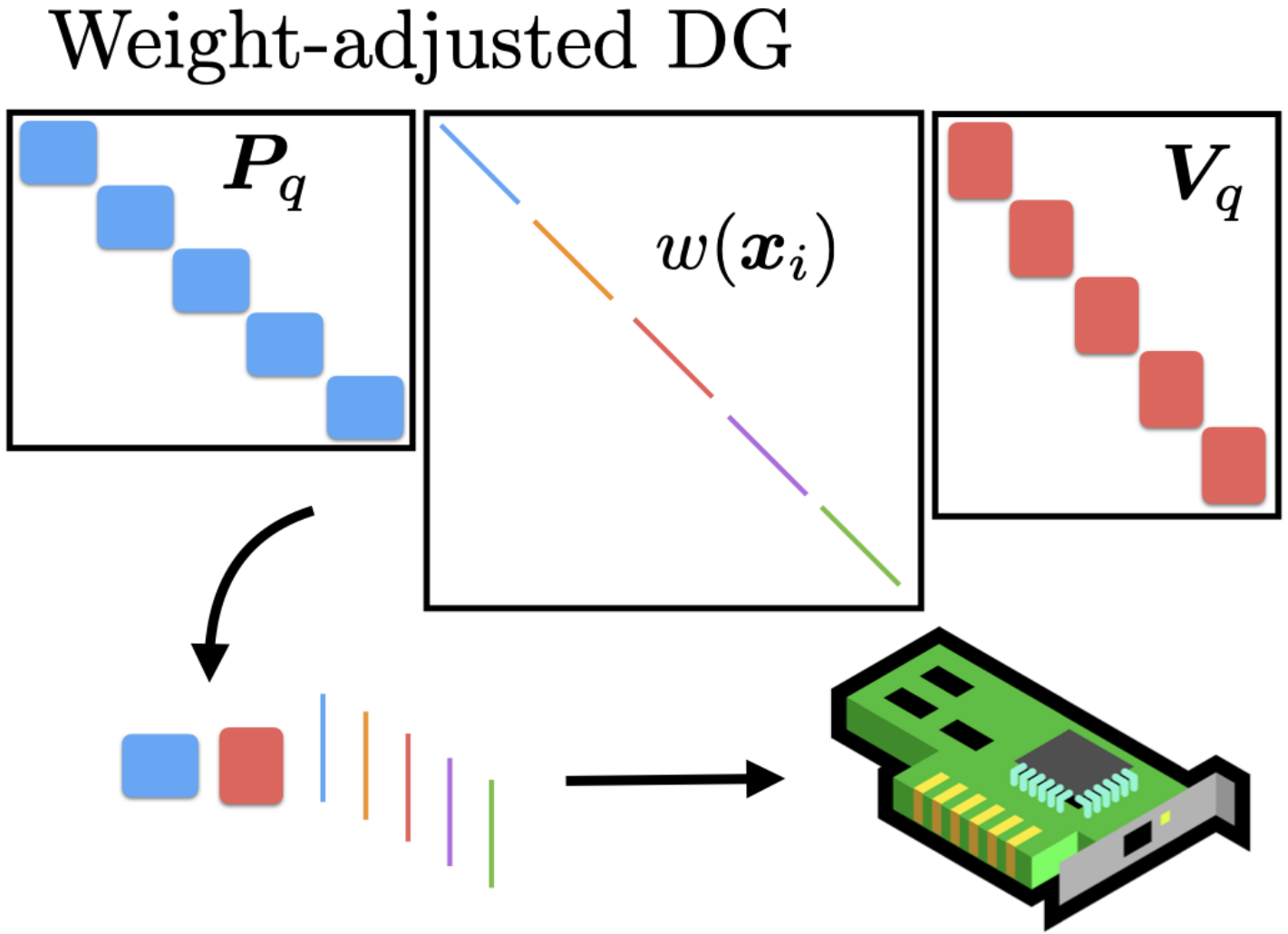

Efficiency on GPUs: reduce memory accesses and data movement!

Outline

1 Weight-adjusted DG (WADG) methods
- High order heterogeneous media
- Curvilinear meshes

2 Elastic and coupled acoustic-elastic media

3 Bernstein-Bezier WADG: high order efficiency

High order DG requires curved representations of geometry

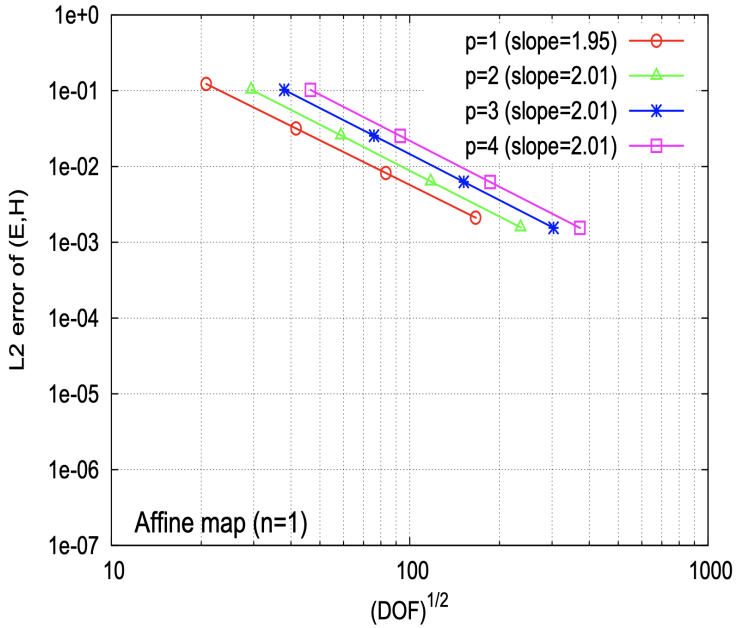

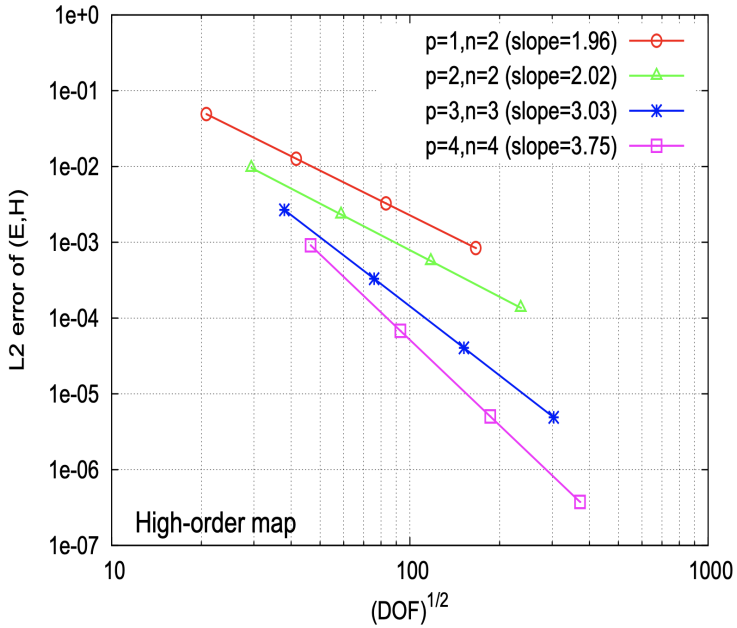

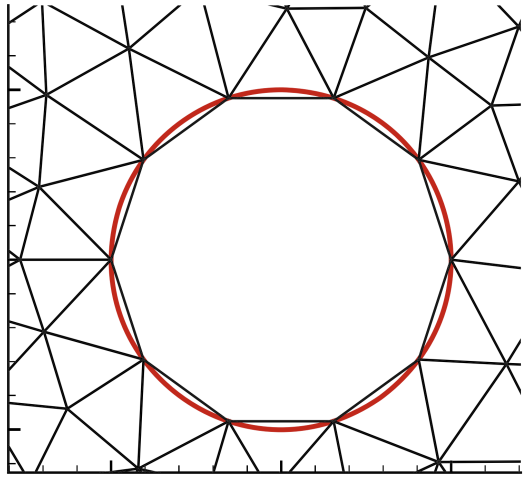

Fahs (2011). Improving accuracy of high-order DG method for time-domain electromagnetics on curvilinear domains.

High order DG requires curved representations of geometry

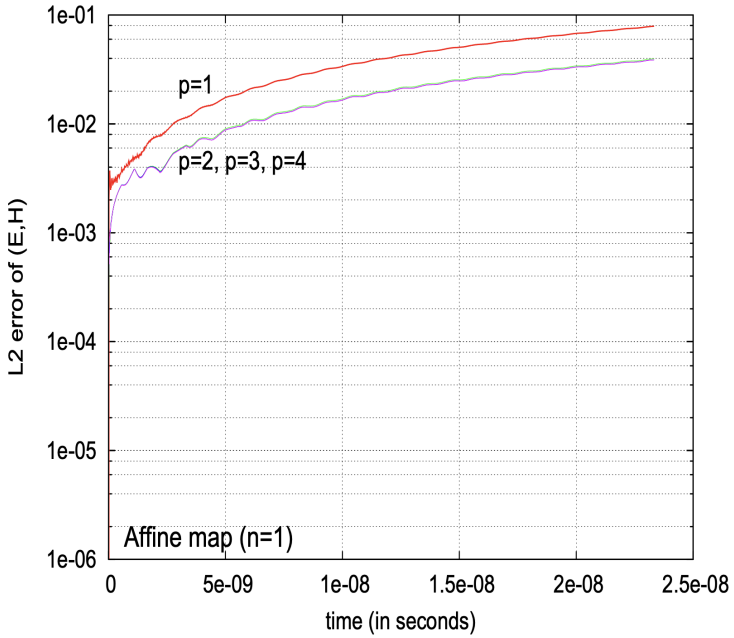

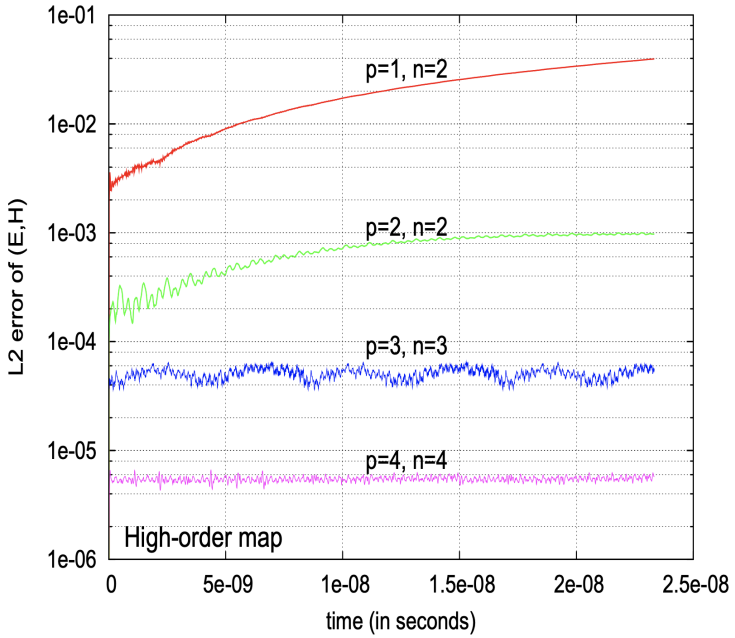

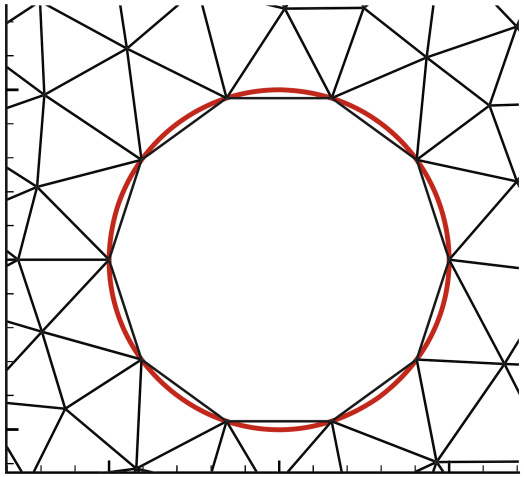

Fahs (2011). Improving accuracy of high-order DG method for time-domain electromagnetics on curvilinear domains.

High order DG requires curved representations of geometry

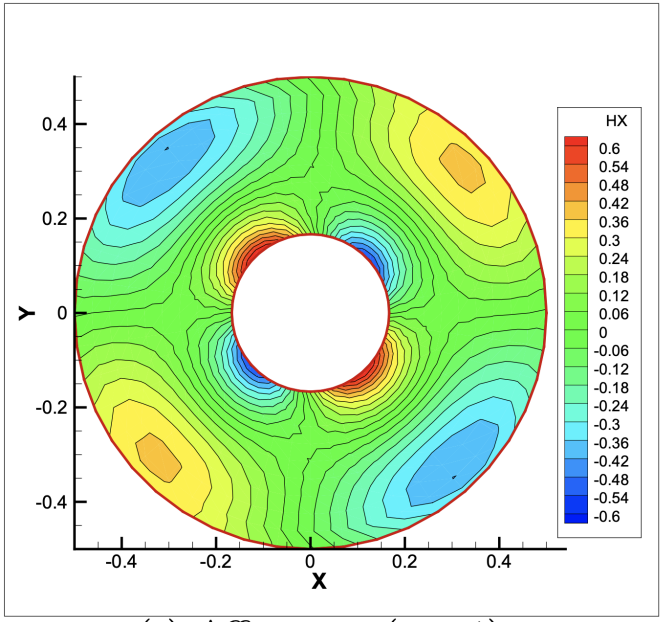

(c) Affine map ($n = 1$).

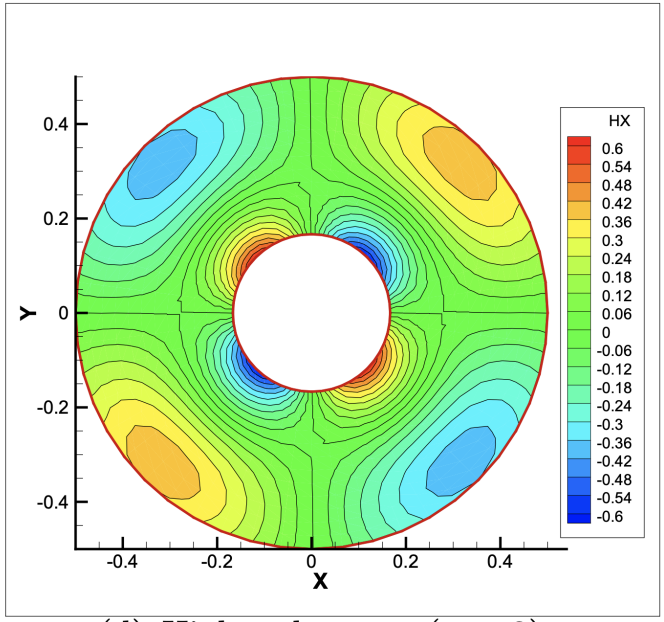

(d) High-order map ($n = 2$).

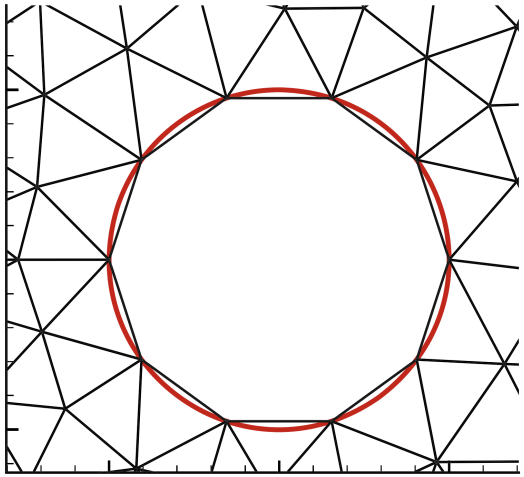

Fahs (2011). Improving accuracy of high-order DG method for time-domain electromagnetics on curvilinear domains.

Weight-adjusted DG for curvilinear meshes

- Weight-adjusted L^2 projection $\tilde{P}_N$ on curved domains

$$\tilde{P}_N(u) := P_N\left(\frac{1}{J}P_N\left(uJ\right)\right).$$

  where P_N is the L^2 projection onto the reference element.

- L^2 error estimates for weight-adjusted projection:

$$\left\|u - \tilde{P}_N u\right\|_{L^2(D^k)} \lesssim \left\|\frac{1}{\sqrt{J}}\right\|_{L^\infty}^2 \|J\|_{W^{N+1,\infty}(D^k)} h^{N+1} \|u\|_{W^{N+1,2}(D^k)}.$$

- High order Sobolev norm of J: implies that convergence can suffer for non-smooth mappings.

Behavior of weight-adjusted L^2 projection

Comparison with L^2 projection and Low-Storage Curvilinear DG

$$\tilde{\phi}_i = \frac{\phi_i}{\sqrt{J}}, \qquad \boldsymbol{M}_{ij} = \int_{D^k} \tilde{\phi}_j \tilde{\phi}_i J = \int_{\widehat{D}} \phi_j \phi_i = \widehat{\boldsymbol{M}}_{ij}.$$

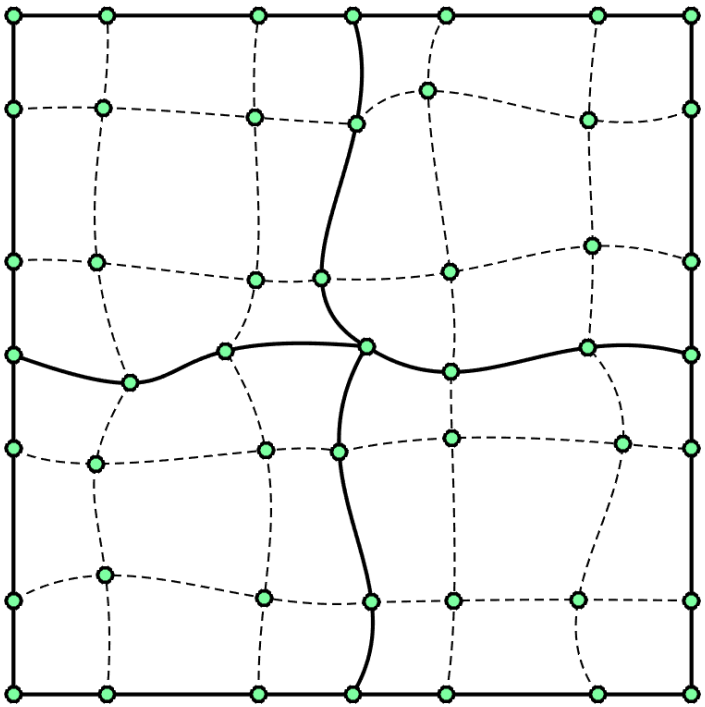

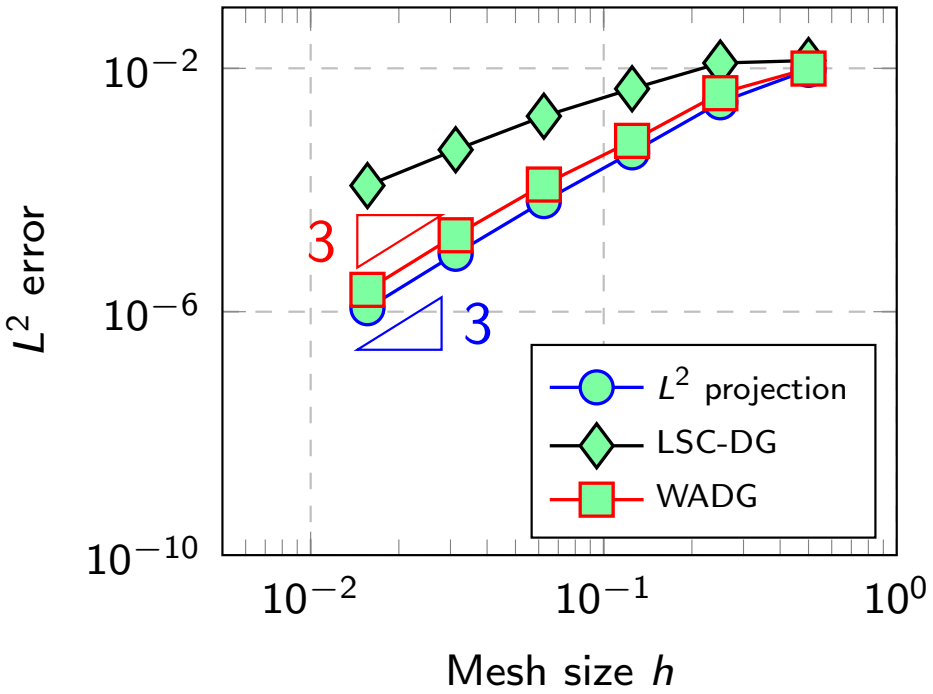

Figure: Curvilinear mesh constructed through random perturbation for $N = 3$.

Behavior of weight-adjusted L^2 projection

Comparison with L^2 projection and Low-Storage Curvilinear DG

$$\tilde{\phi}_i = \frac{\phi_i}{\sqrt{J}}, \qquad \boldsymbol{M}_{ij} = \int_{D^k} \tilde{\phi}_j \tilde{\phi}_i J = \int_{\widehat{D}} \phi_j \phi_i = \widehat{\boldsymbol{M}}_{ij}.$$

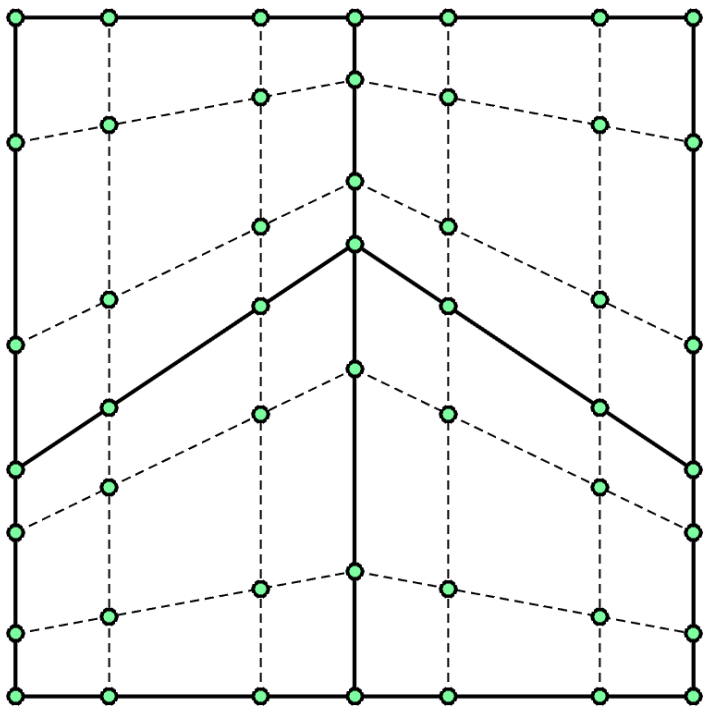

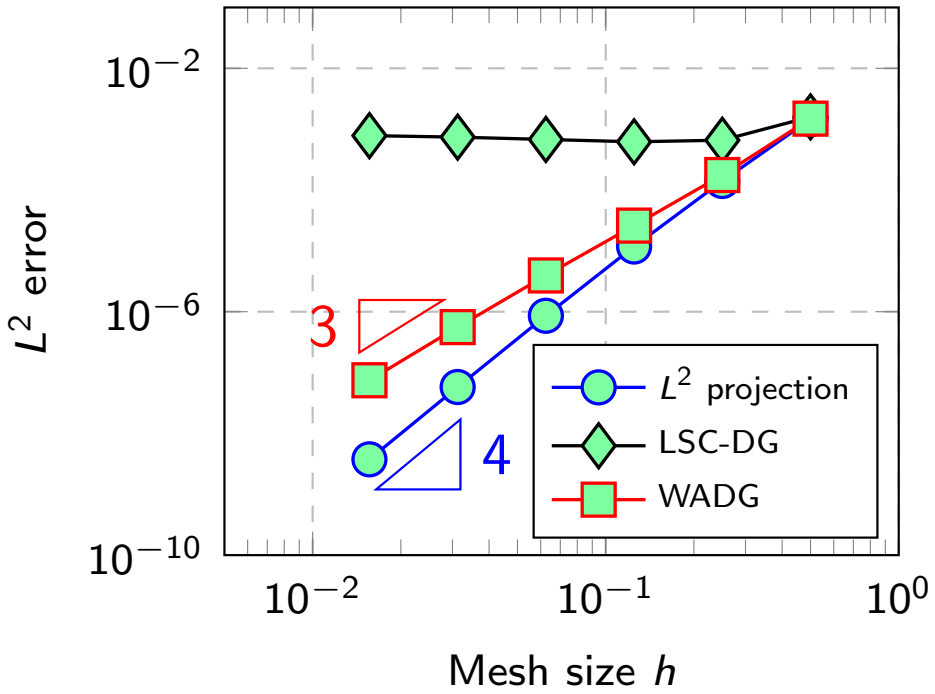

Figure: Arnold-type mesh with $\|J\|_{W^{N+1,\infty}} = O(h^{-1})$ for $N = 3$.

Behavior of weight-adjusted L^2 projection

High order convergence slowed by growth of $\|J\|_{W^{N+1,\infty}} = O(h^N)$.

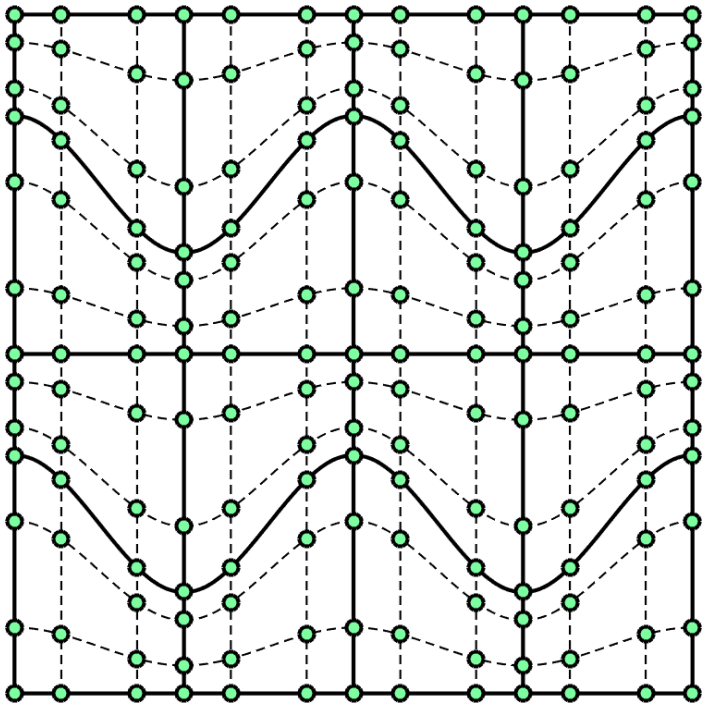

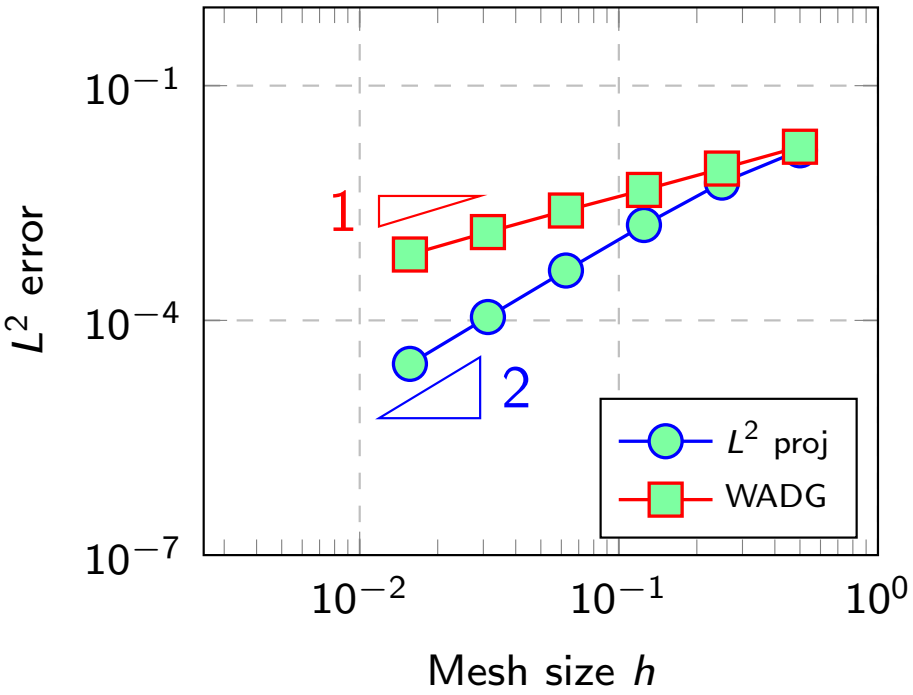

Figure: Moderately warped curved Arnold-type mesh for $N = 3$.

Behavior of weight-adjusted L^2 projection

High order convergence is stalled by growth of $\|J\|_{W^{N+1,\infty}} = O(h^{N+1})$.

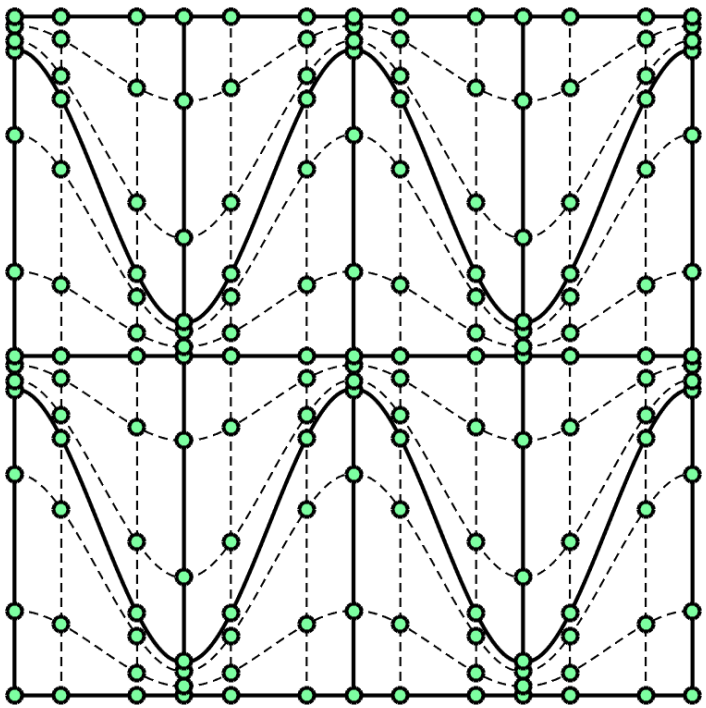

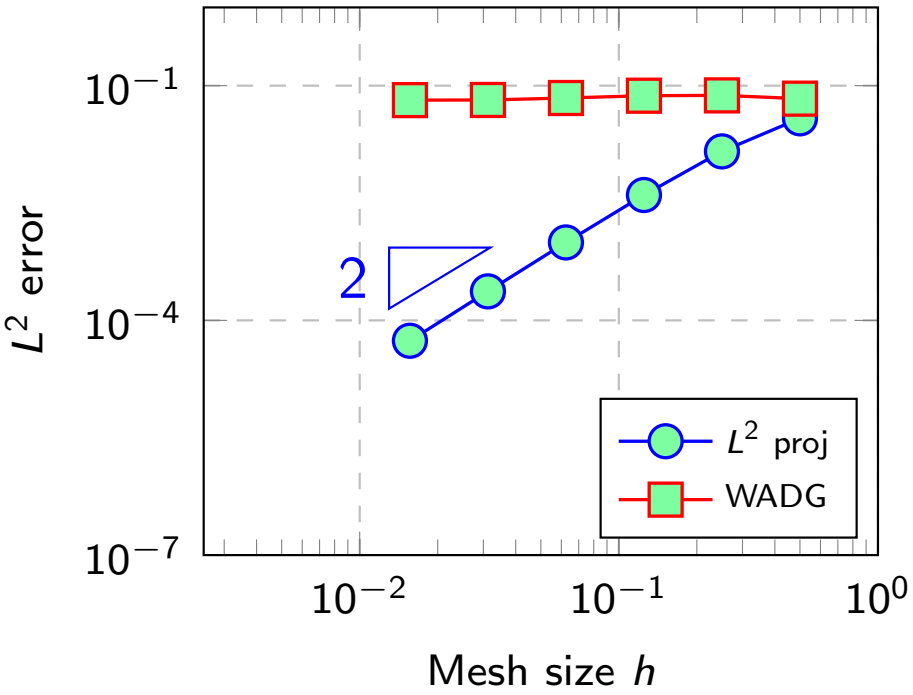

Figure: Heavily warped curved Arnold-type mesh for $N = 3$.

Curvilinear meshes: two-dimensional verification

Energy stability: quadrature-based skew-symmetric formulation.

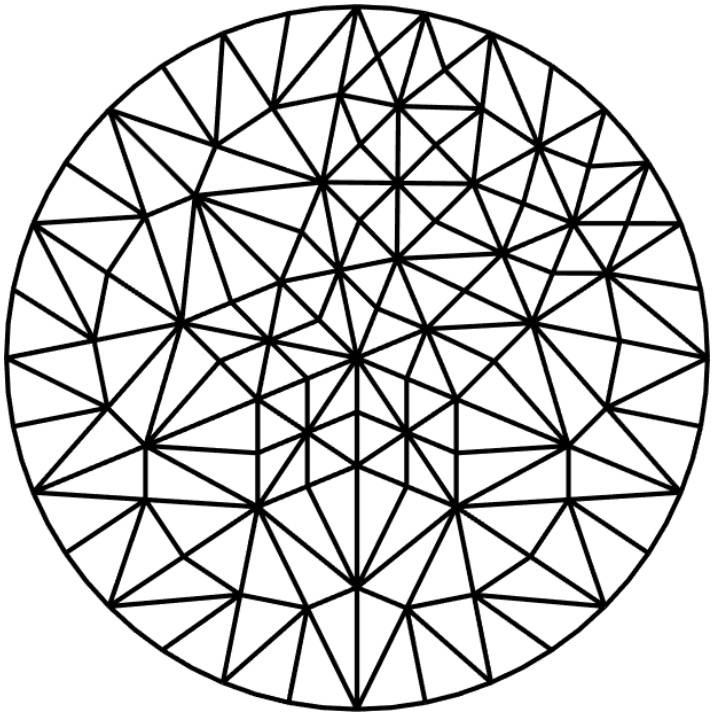

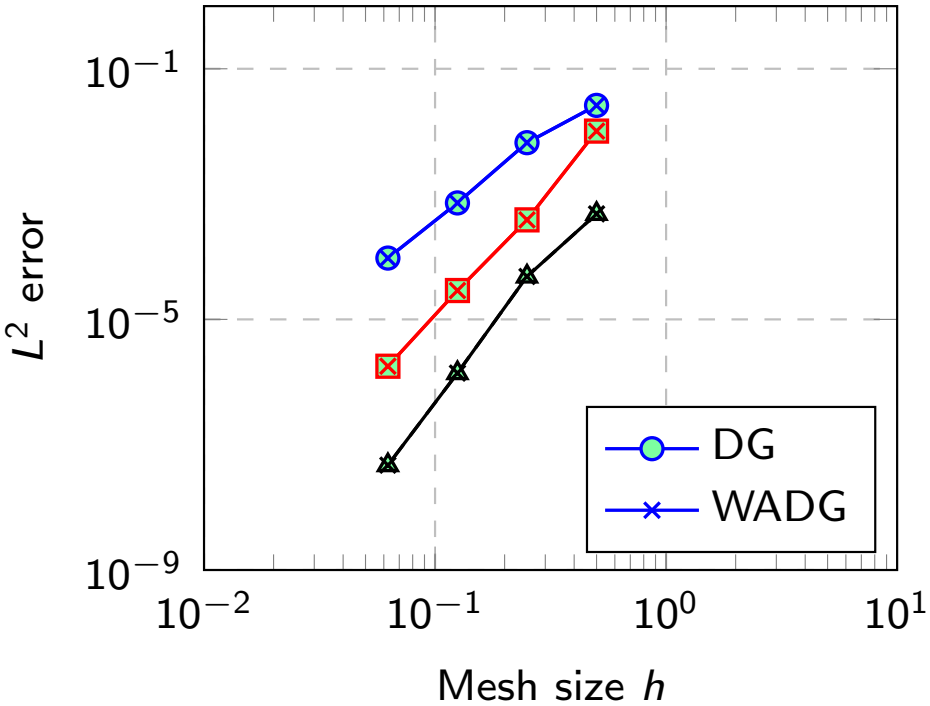

(a) L^2 errors for $N = 2, 3, 4$

Figure: Optimal L^2 convergence rates observed for curvilinear meshes.

Curvilinear meshes: DG eigenvalues (circular domain)

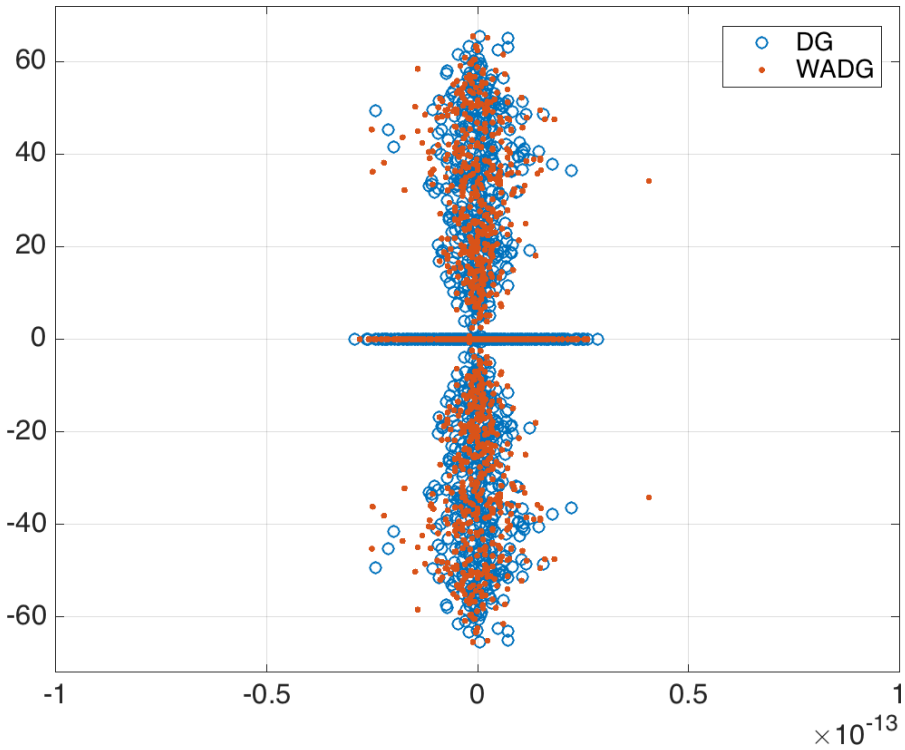

(a) Central fluxes

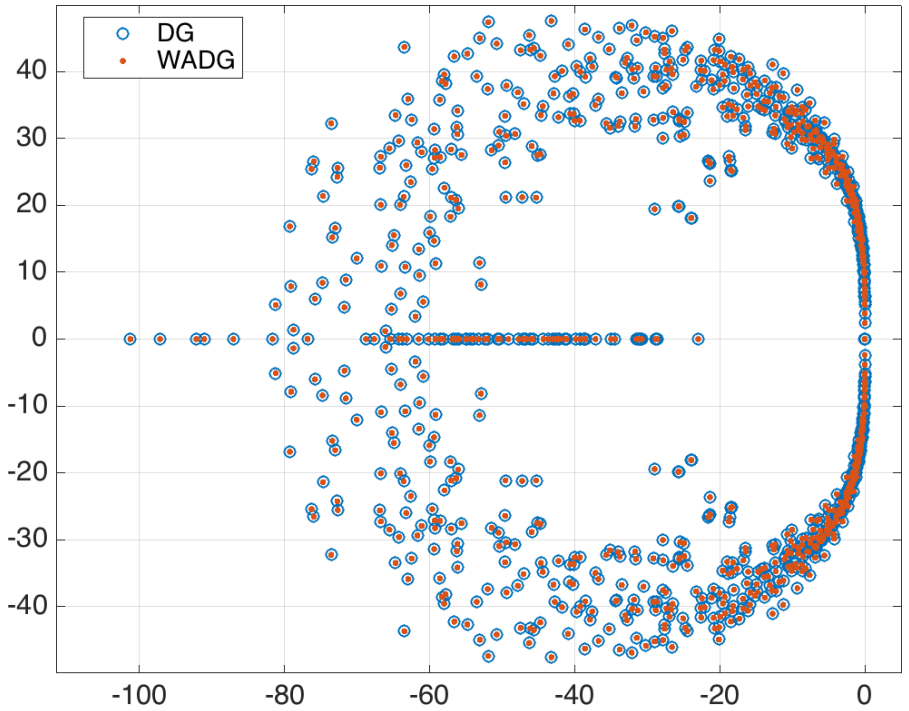

(b) Upwind fluxes

Curved meshes + heterogeneous media

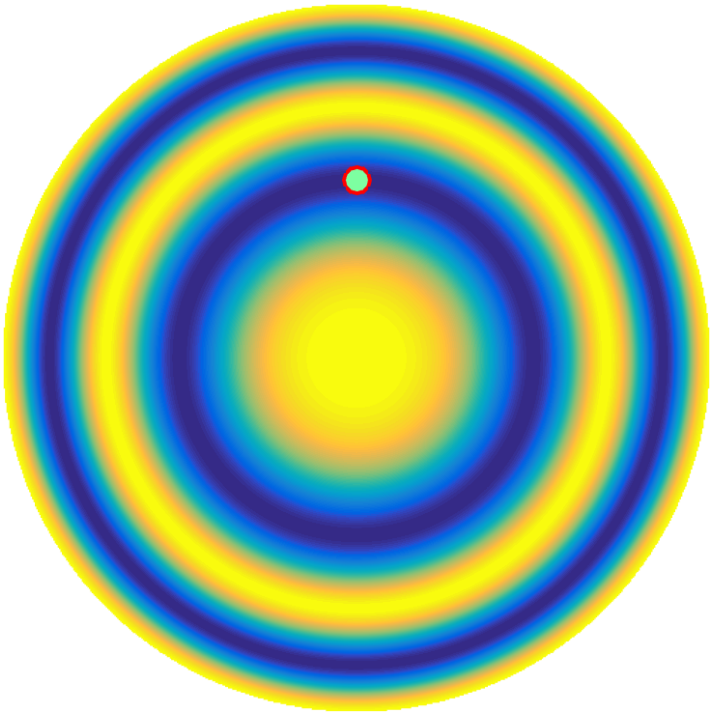

(a) Wavespeed $c^2(\boldsymbol{x})$

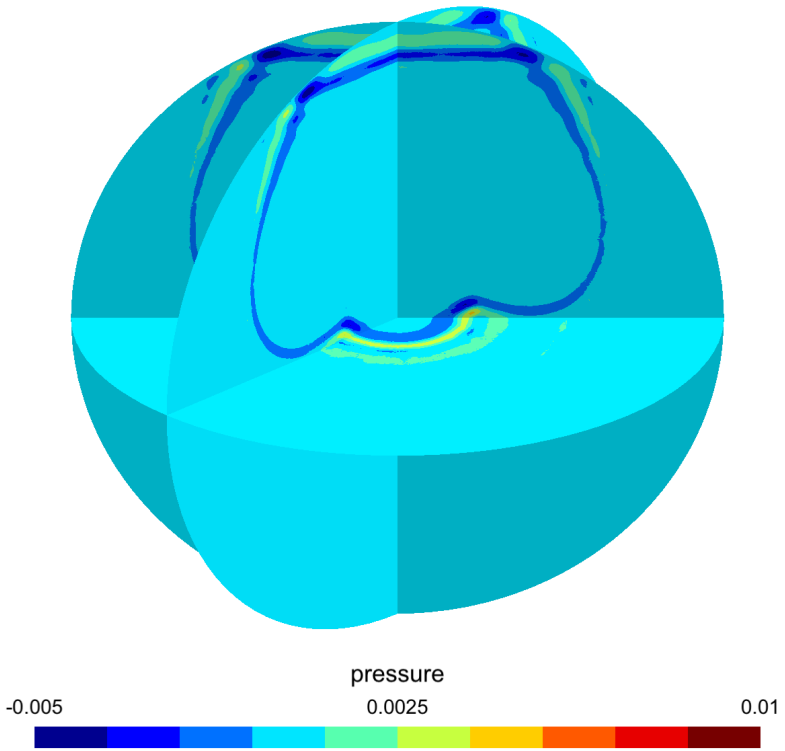

(b) Pressure isovalues at $t = .6$

Can incorporate heterogeneous media with curved elements at no additional cost.

Restoring Kronecker structure to $\boldsymbol{M}^{-1}$

- Explicit time-stepping for isogeometric analysis is inefficient due to loss of Kronecker product structure in spline mass matrix inverses.
- WADG recovers tensor product in application of $\boldsymbol{M}_{1/J}$, $\widehat{\boldsymbol{M}}^{-1}$

$$\boldsymbol{M}_J^{-1} \approx \widehat{\boldsymbol{M}}^{-1} \boldsymbol{M}_{1/J} \widehat{\boldsymbol{M}}^{-1}$$
$$\widehat{\boldsymbol{M}}^{-1} = \widehat{\boldsymbol{M}}_{1\mathrm{D}}^{-1} \otimes \widehat{\boldsymbol{M}}_{1\mathrm{D}}^{-1} \otimes \widehat{\boldsymbol{M}}_{1\mathrm{D}}^{-1}.$$

- Maintains **provable** energy stability for general geometric mappings.

Chan, Evans (2018). Multi-patch DG-IGA for wave propagation: explicit time-stepping and efficient mass matrix inversion.

Outline

1 Weight-adjusted DG (WADG) methods
- High order heterogeneous media
- Curvilinear meshes

2 Elastic and coupled acoustic-elastic media

3 Bernstein-Bezier WADG: high order efficiency

Matrix-valued weights and elastic wave propagation

- Symmetric hyperbolic system: velocity $\boldsymbol{v}$, stress $\boldsymbol{\sigma} = \mathrm{vec}(\boldsymbol{S})$ with $\boldsymbol{\sigma} = (\sigma_{xx}, \sigma_{yy}, \sigma_{zz}, \sigma_{yz}, \sigma_{xz}, \sigma_{xy})^T$.

$$\rho \frac{\partial \boldsymbol{v}}{\partial t} = \sum_{i=1}^{d} \boldsymbol{A}_i^T \frac{\partial \boldsymbol{\sigma}}{\partial \boldsymbol{x}_i}, \qquad \boldsymbol{C}^{-1} \frac{\partial \boldsymbol{\sigma}}{\partial t} = \sum_{i=1}^{d} \boldsymbol{A}_i \frac{\partial \boldsymbol{v}}{\partial \boldsymbol{x}_i}.$$

- Factoring out the constitutive stiffness tensor $\boldsymbol{C}$ results in simple and spatially constant matrices $\boldsymbol{A}_i$.

$$\boldsymbol{C} = \underbrace{\begin{pmatrix} 2\mu+\lambda & \lambda & \lambda & & & \\ \lambda & 2\mu+\lambda & \lambda & & & \\ \lambda & \lambda & 2\mu+\lambda & & & \\ & & & \mu & & \\ & & & & \mu & \\ & & & & & \mu \end{pmatrix}}_{\text{for isotropic media}}, \quad \boldsymbol{A}_1 = \begin{pmatrix} 1 & 0 & 0 \\ 0 & 0 & 0 \\ 0 & 0 & 0 \\ 0 & 0 & 0 \\ 0 & 0 & 1 \\ 0 & 1 & 0 \end{pmatrix}.$$

Hughes and Marsden 1978. Classical elastodynamics as a linear symmetric hyperbolic system.

DG formulation for elasticity

$$\int_{D^k} \boldsymbol{C}^{-1} \frac{\partial \boldsymbol{\sigma}}{\partial t} \cdot \boldsymbol{q} = \int_{D^k} \sum_{i=1}^{d} \boldsymbol{A}_i \frac{\partial \boldsymbol{v}}{\partial \boldsymbol{x}_i} \boldsymbol{q} + \frac{1}{2} \int_{\partial D^k} \left(\boldsymbol{A}_n [\![\boldsymbol{v}]\!] + \tau_\sigma \boldsymbol{A}_n \boldsymbol{A}_n^T [\![\boldsymbol{\sigma}]\!] \right) \boldsymbol{q},$$

$$\int_{D^k} \rho \frac{\partial \boldsymbol{v}}{\partial t} \cdot \boldsymbol{w} = \int_{D^k} \sum_{i=1}^{d} \boldsymbol{A}_i^T \frac{\partial \boldsymbol{\sigma}}{\partial \boldsymbol{x}_i} \boldsymbol{w} + \frac{1}{2} \int_{\partial D^k} \left(\boldsymbol{A}_n^T [\![\boldsymbol{\sigma}]\!] + \tau_v \boldsymbol{A}_n^T \boldsymbol{A}_n [\![\boldsymbol{v}]\!] \right) \boldsymbol{w}.$$

- Analogous to acoustics: numerical fluxes independent of media!
- Energy stability (penalty weakly enforces continuity conditions):

$$\sum_{D^k} \frac{1}{2} \frac{\partial}{\partial t} \int_{D^k} \rho |\boldsymbol{v}|^2 + \boldsymbol{\sigma}^T \boldsymbol{C}^{-1} \boldsymbol{\sigma} =$$

$$- \sum_{\text{faces}} \int_f \frac{\tau_{\boldsymbol{v}}}{2} |\boldsymbol{A}_n [\![\boldsymbol{v}]\!]|^2 + \frac{\tau_{\boldsymbol{\sigma}}}{2} \left| \boldsymbol{A}_n^T [\![\boldsymbol{\sigma}]\!] \right|^2 \leq 0.$$

- $\tau_v, \tau_\sigma > 0$ penalizes normal jumps $[\![\boldsymbol{v}]\!] \cdot \boldsymbol{n} \approx 0$, $[\![\boldsymbol{S}]\!] \cdot \boldsymbol{n} \approx 0$.

Semi-discrete system: matrix-valued weighted

- Matrix-weighted mass matrix: let $\boldsymbol{W} \in \mathbb{R}^{d \times d}$ be SPD with entries w_{ij}

$$\boldsymbol{M}_{\boldsymbol{W}} = \begin{pmatrix} \boldsymbol{M}_{w_{11}} & \cdots & \boldsymbol{M}_{w_{1d}} \\ \vdots & \ddots & \vdots \\ \boldsymbol{M}_{w_{d1}} & \cdots & \boldsymbol{M}_{w_{dd}} \end{pmatrix}$$

- Semi-discrete DG formulation involves $\boldsymbol{C}^{-1}$-weighted mass matrix

$$\boldsymbol{M}_{\boldsymbol{C}^{-1}} \frac{\partial \boldsymbol{\Sigma}}{\partial t} = \text{stress right hand side}$$

$$\boldsymbol{M}_{\rho \boldsymbol{I}} \frac{\partial \boldsymbol{V}}{\partial t} = \text{velocity right hand side}$$

Weight-adjusted DG: matrix-valued weights

- Matrix-weighted mass matrix large, hard to invert

$$\boldsymbol{M}_{\boldsymbol{C}^{-1}} = \begin{pmatrix} \boldsymbol{M}_{\boldsymbol{C}_{11}^{-1}} & \dots & \boldsymbol{M}_{\boldsymbol{C}_{1d}^{-1}} \\ \vdots & \ddots & \vdots \\ \boldsymbol{M}_{\boldsymbol{C}_{d1}^{-1}} & \dots & \boldsymbol{M}_{\boldsymbol{C}_{dd}^{-1}} \end{pmatrix}$$

- Weight-adjusted approximation for $\boldsymbol{C}^{-1}$ decouples each component

$$\boldsymbol{M}_{\boldsymbol{C}^{-1}}^{-1} \approx \left(\boldsymbol{I} \otimes \boldsymbol{M}^{-1}\right) \boldsymbol{M}_{\boldsymbol{C}} \left(\boldsymbol{I} \otimes \boldsymbol{M}^{-1}\right).$$

- Evaluate RHS components at quadrature points, apply $\boldsymbol{C}(\boldsymbol{x}_i)$ to component vectors at quadrature points, project back to polynomials.

- Recovers Kronecker product $\boldsymbol{M}_{\boldsymbol{C}^{-1}}^{-1} = \boldsymbol{C} \otimes \boldsymbol{M}^{-1}$ for constant $\boldsymbol{C}^{-1}$.

Energy stability and DG spectra

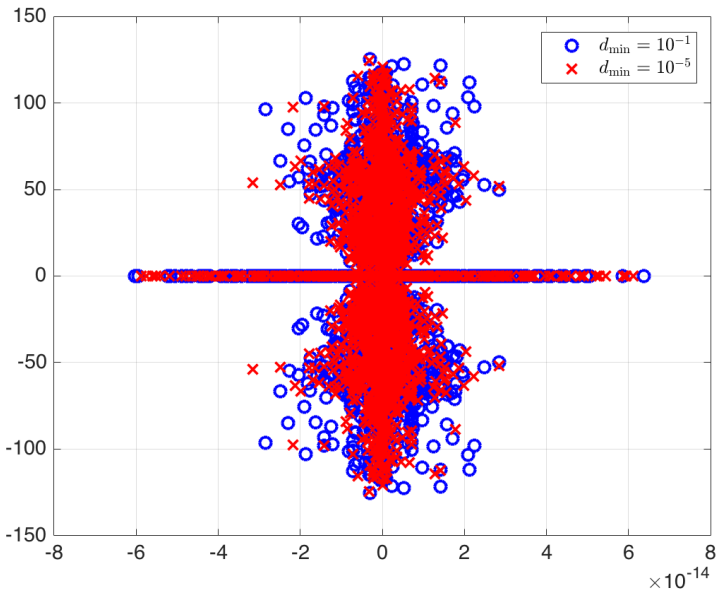

(a) Central flux ($\tau_v, \tau_\sigma = 0$)

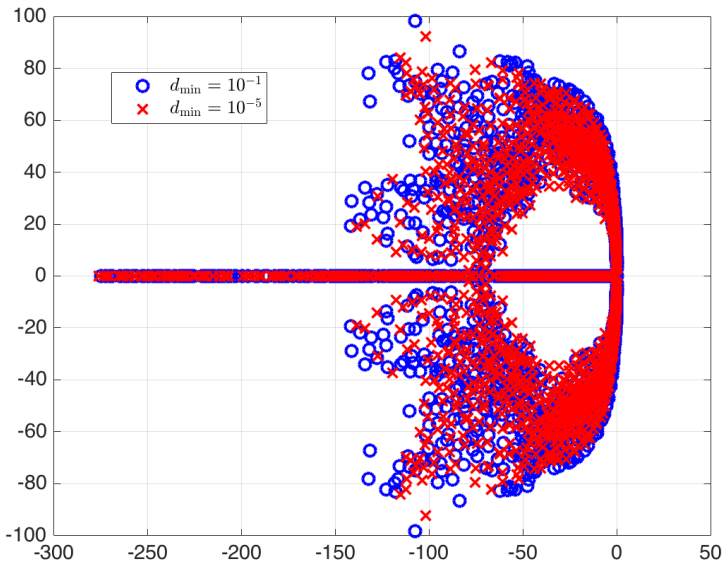

(b) Penalty flux ($\tau_v, \tau_\sigma = 1$)

Figure: DG spectra with random heterogeneities at each quadrature point.

- Guaranteed energy stability for both energy conservative and energy dissipative numerical interface fluxes.
- CFL can be improved by setting $\tau_\sigma \approx 1/\left\|\boldsymbol{C}\right\|$, $\tau_v \approx \left\|\rho\right\|$

Elastic wave propagation: convergence

- Convergence for harmonic oscillation, Rayleigh, Lamb, and Stoneley waves: between $O(h^{N+1})$ and $O(h^{N+1/2})$.
- $\boldsymbol{\sigma}$ error grows as $\left\|\boldsymbol{C}^{-1}\right\| \to \infty$ (e.g. incompressible limit $\lambda/\mu \to \infty$).

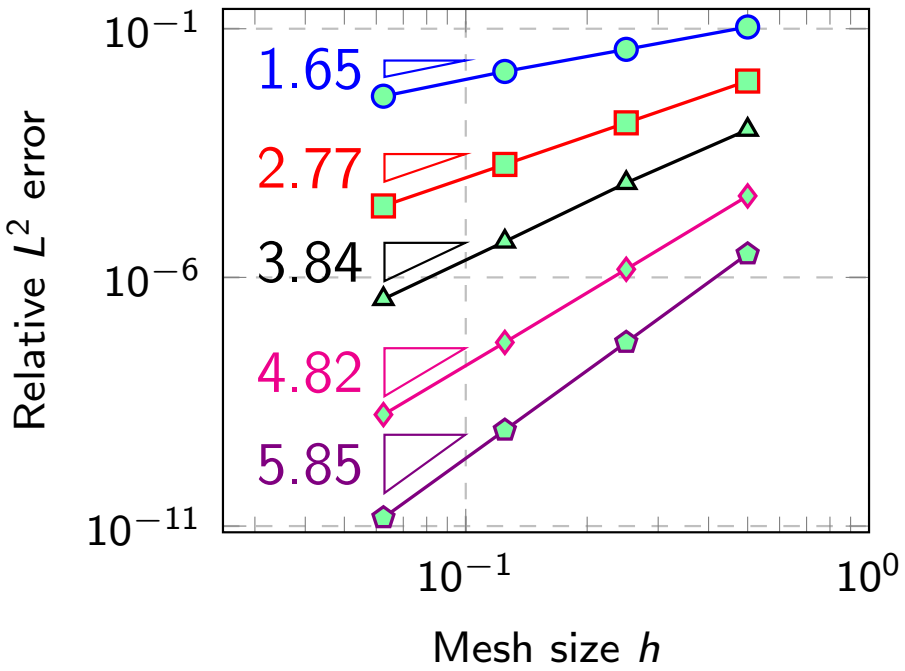

(a) L^2 errors (Stoneley wave)

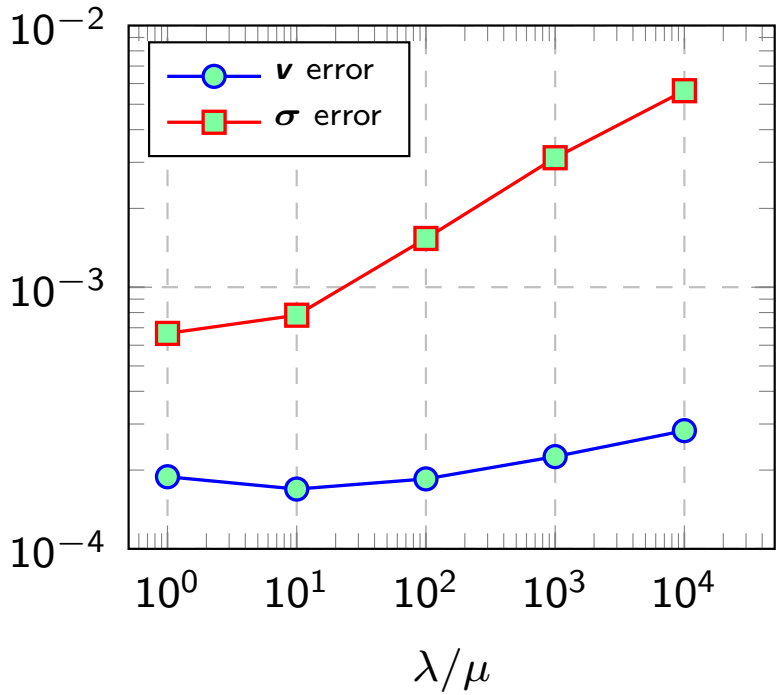

(b) $\left\|\boldsymbol{C}^{-1}\right\| \to \infty$, $N = 3, h = 1/8$.

Elastic wave propagation: stiff inclusion

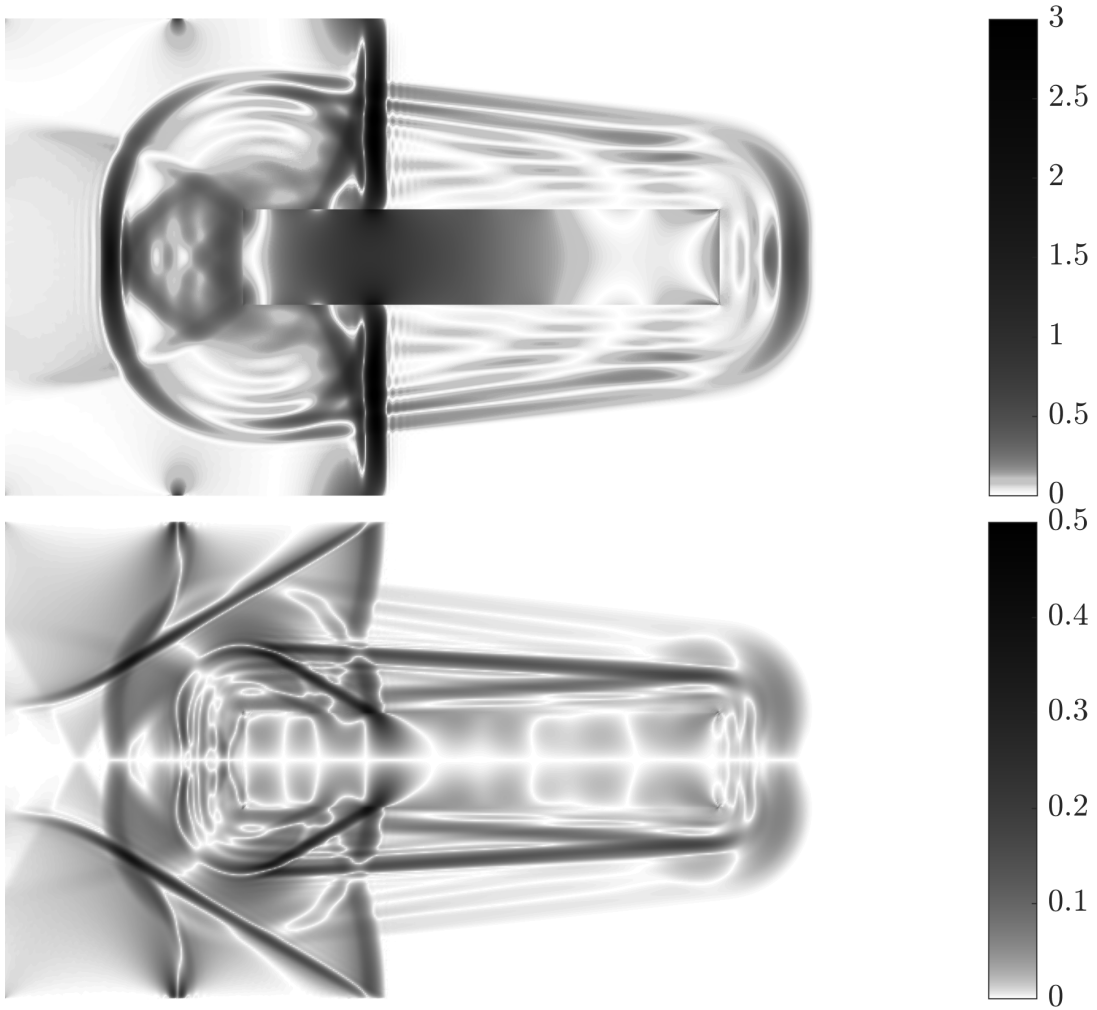

Figure: $\mathrm{tr}(\boldsymbol{\sigma})$ and $\boldsymbol{\sigma}_{xy}$ for stiff inclusion with $N = 5$, $h \approx 1/50$.

Simple to incorporate anisotropic media

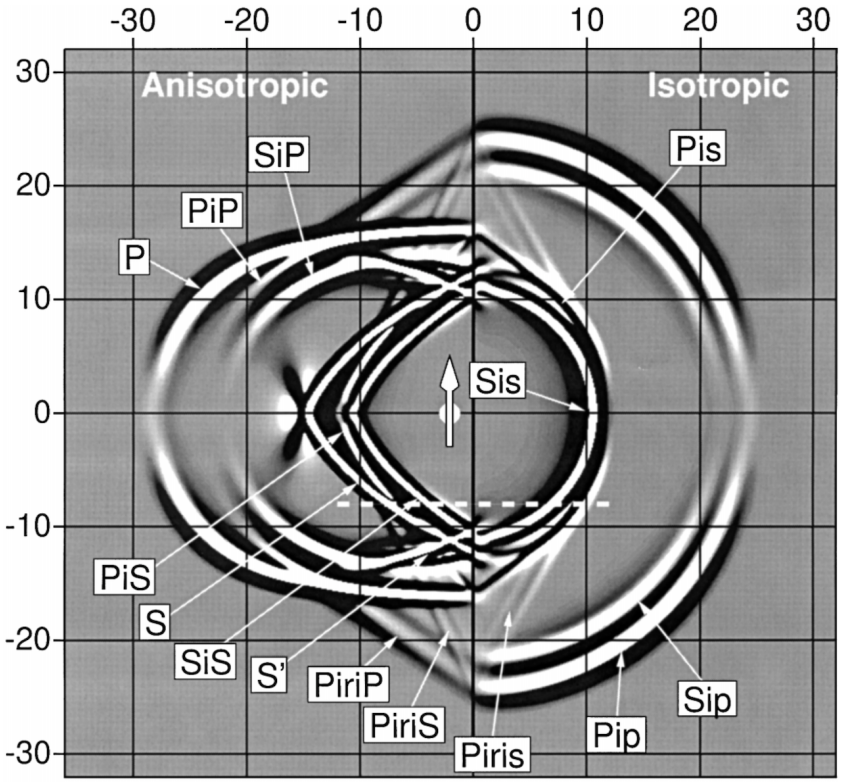

(a) Reference solution

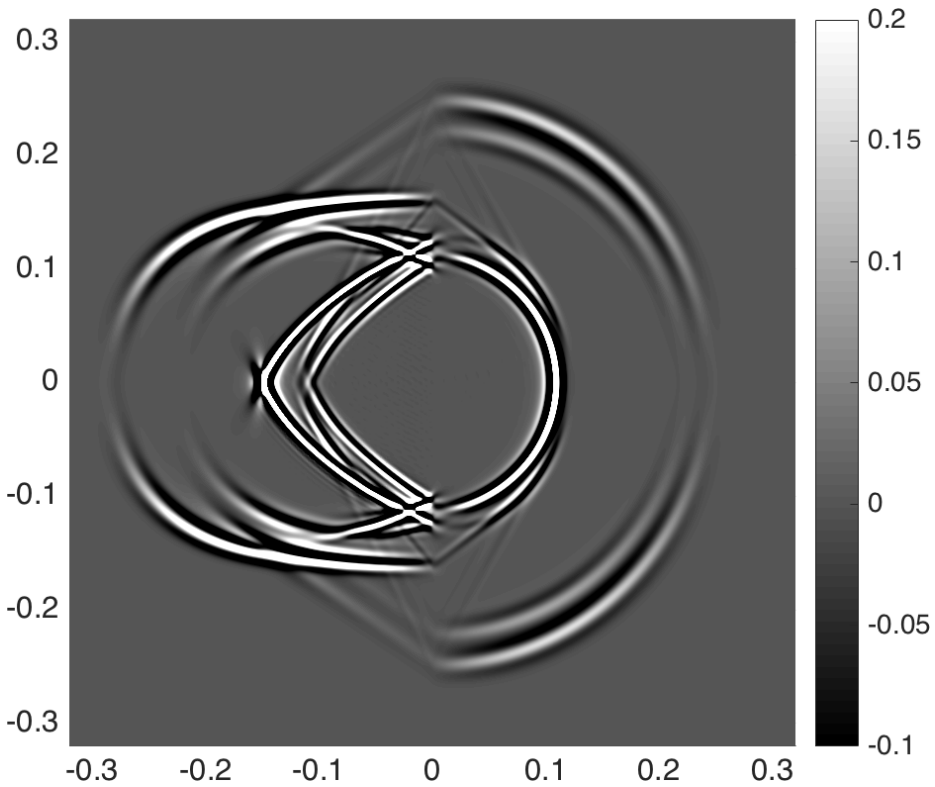

(b) WADG solution

Figure: Anisotropic media simply involves modifying the definition of $\boldsymbol{C}$.

Komatitsch, Barnes, Tromp (2000). *Simulation of anisotropic wave propagation based upon a spectral element method.*

Chan (2018). Weight-adjusted DG methods: matrix-valued weights and elastic wave prop. in heterogeneous media.

Elastic wave propagation: 3D isotropic media

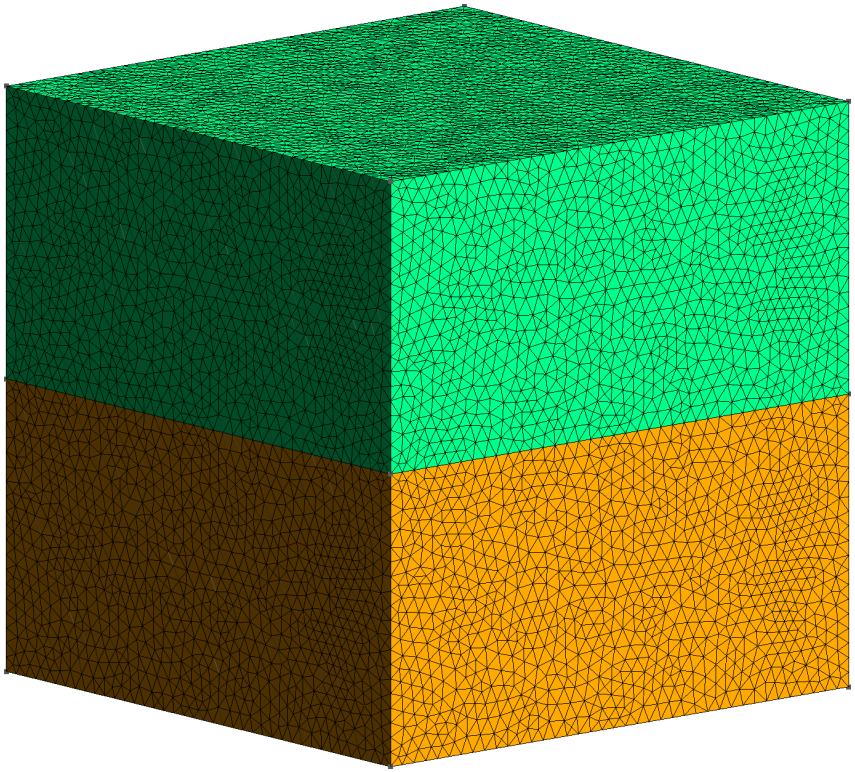

(a) Computational mesh

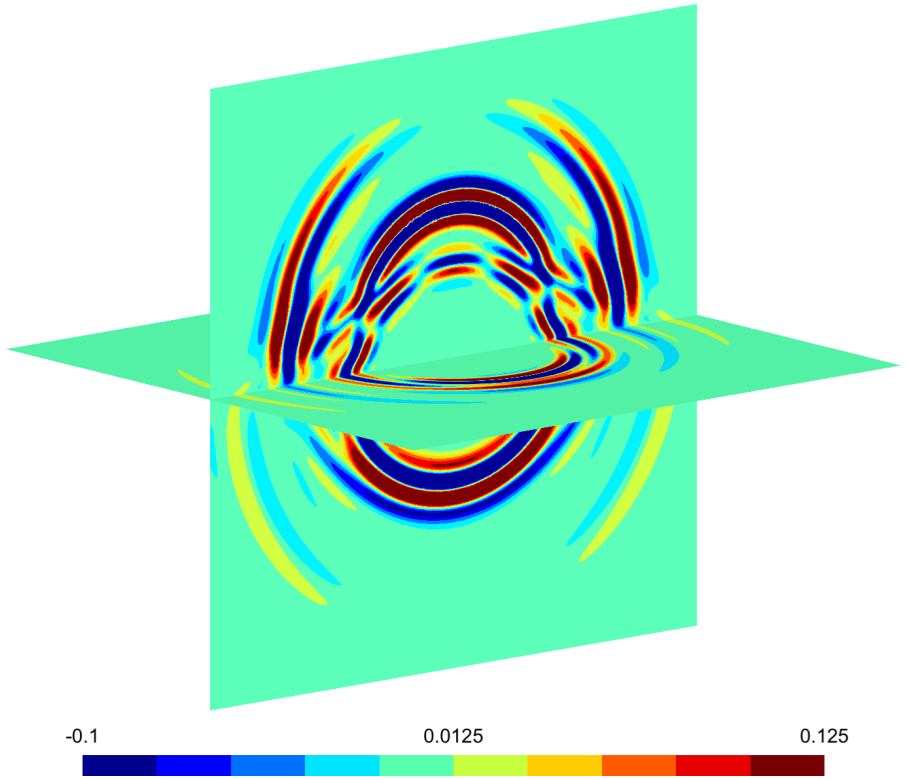

(b) Homogeneous isotropic media

Figure: $\mathrm{tr}(\boldsymbol{\sigma})$ with $\mu(\boldsymbol{x}) = 1 + H(y) + \frac{1}{2}\cos(3\pi x)\cos(3\pi y)\cos(3\pi z)$, $N = 5$.

Elastic wave propagation: 3D isotropic media

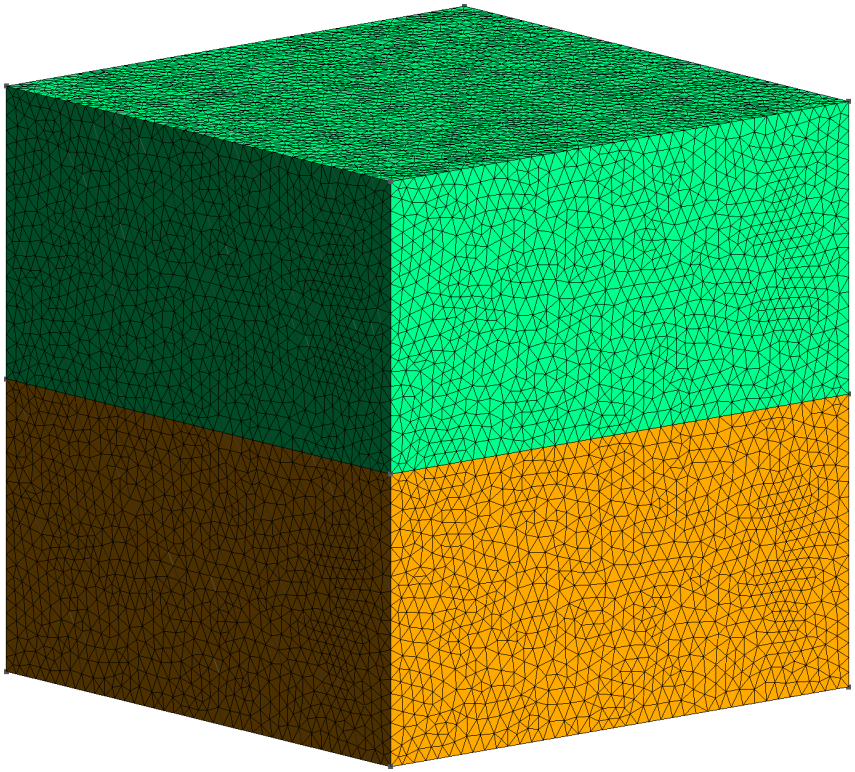

(a) Computational mesh

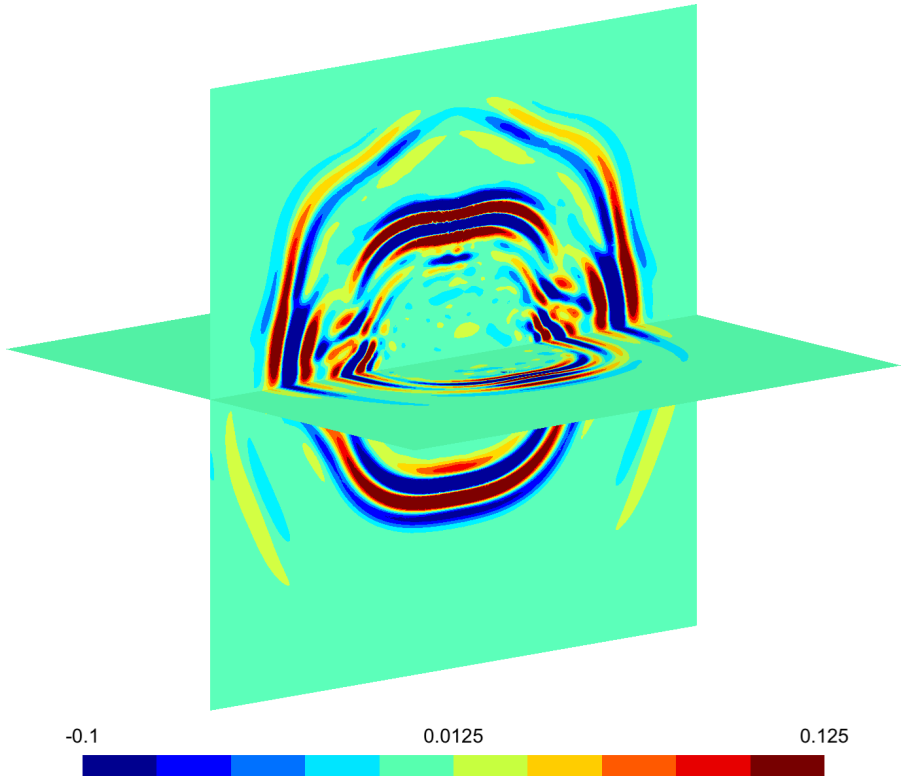

(b) Piecewise constant $\boldsymbol{C}(\boldsymbol{x})$

Figure: $\mathrm{tr}(\boldsymbol{\sigma})$ with $\mu(\boldsymbol{x}) = 1 + H(y) + \frac{1}{2}\cos(3\pi x)\cos(3\pi y)\cos(3\pi z)$, $N = 5$.

Elastic wave propagation: 3D isotropic media

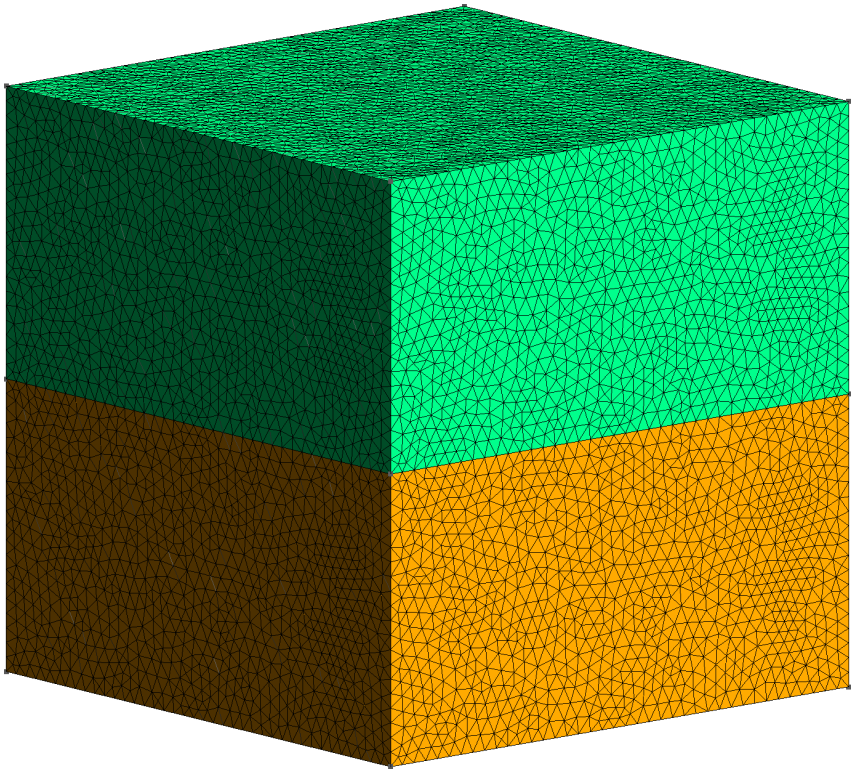

(a) Computational mesh

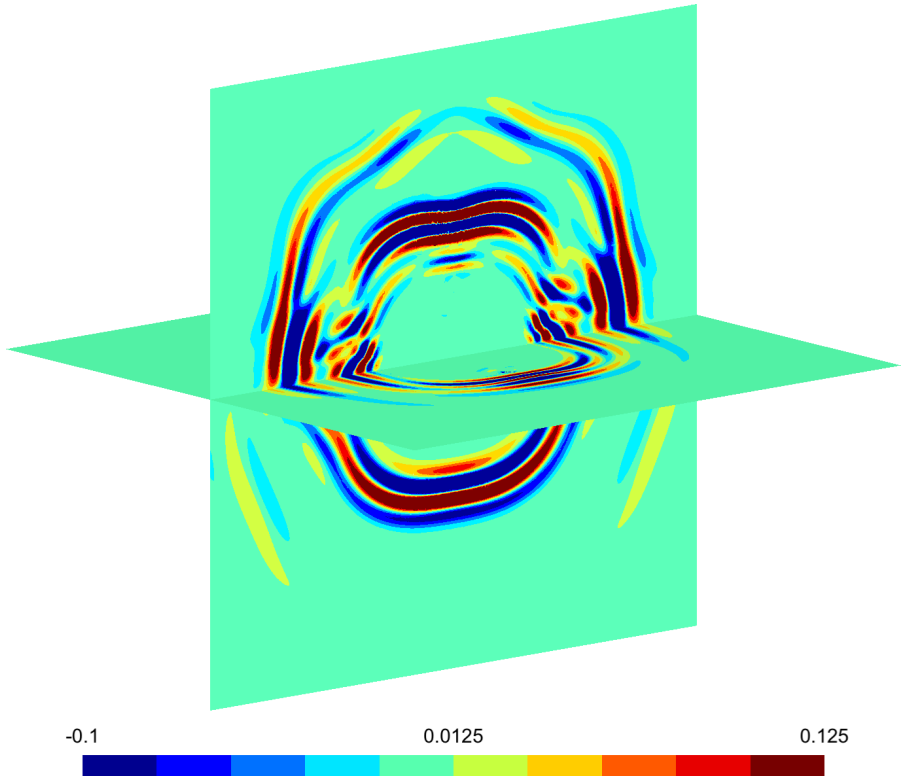

(b) High order $\boldsymbol{C}(\boldsymbol{x})$

Figure: $\mathrm{tr}(\boldsymbol{\sigma})$ with $\mu(\boldsymbol{x}) = 1 + H(y) + \frac{1}{2}\cos(3\pi x)\cos(3\pi y)\cos(3\pi z)$, $N = 5$.

Energy stable acoustic-elastic coupling (with Guo)

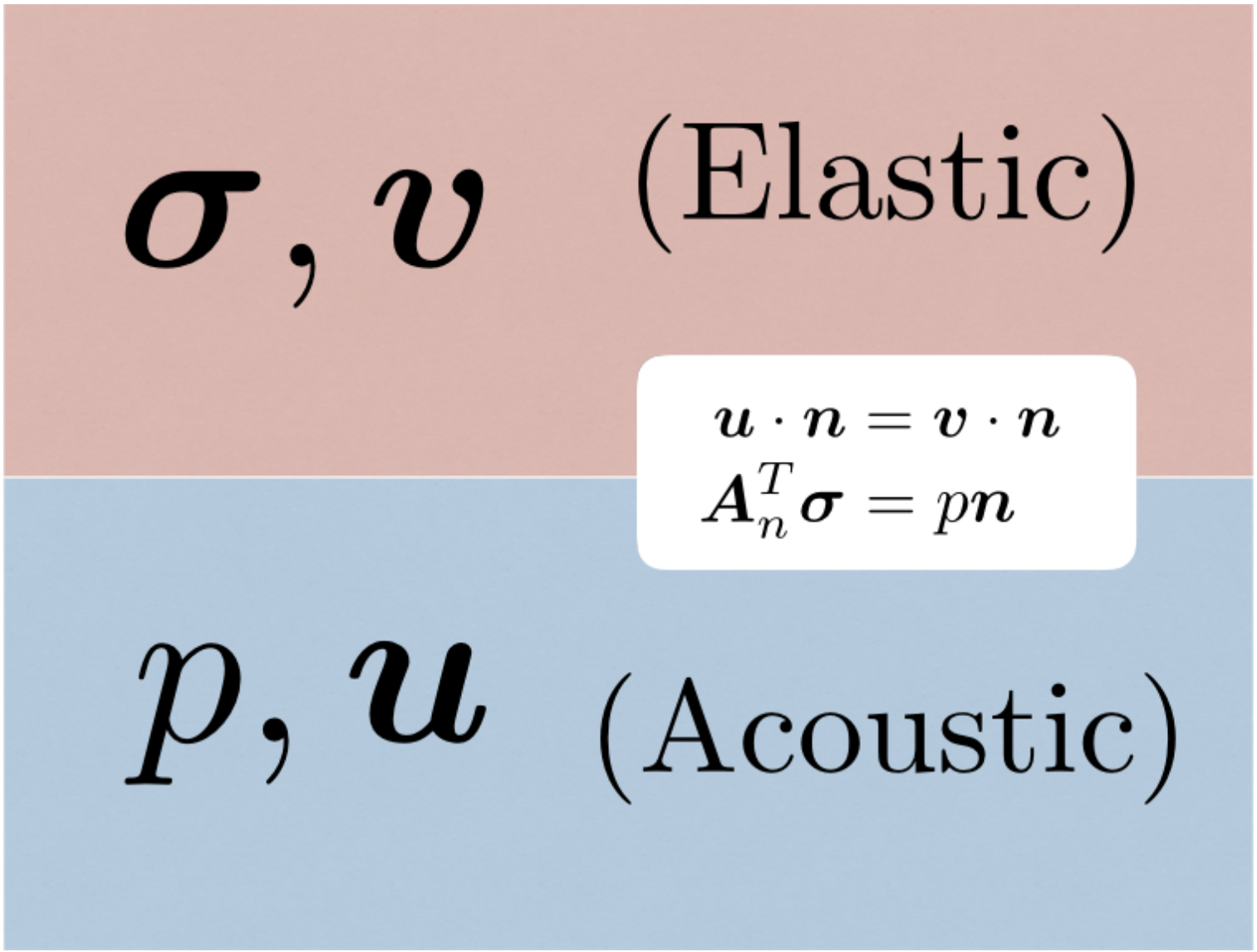

Energy stable acoustic-elastic coupling (with Guo)

$$(\mathfrak{F}\boldsymbol{q})^* = \mathfrak{F}^-\boldsymbol{q}^- + \frac{\boldsymbol{n}\cdot[\![\boldsymbol{S}]\!] + \rho^+ c_p^+ [\![\boldsymbol{v}]\!]}{\rho^+ c_p^+ + \rho^- c_p^-} \begin{pmatrix} \boldsymbol{n}\otimes\boldsymbol{n} \\ \rho^- c_p^- \boldsymbol{n} \end{pmatrix}.$$

$$\begin{aligned}(\mathfrak{F}\boldsymbol{q})^* = \mathfrak{F}^-\boldsymbol{q}^- &+ \frac{c_p^- c_p^+ \boldsymbol{n}\cdot[\![\boldsymbol{S}]\!] + c_p^-(\lambda^+ + 2\mu^+)[\![\boldsymbol{v}]\!]}{c_p^+(\lambda^- + 2\mu^-) + c_p^-(\lambda^+ + 2\mu^+)} \begin{pmatrix} \boldsymbol{n}\otimes\boldsymbol{n} \\ \rho^- c_p^- \boldsymbol{n} \end{pmatrix} + \left(\frac{c_s^- c_s^+}{\mu^+ c_s^- + \mu^- c_s^+} \boldsymbol{s}\cdot[\![\boldsymbol{S}]\!] + \frac{c_s^- \mu^+}{\mu^+ c_s^- + \mu^- c_s^+} \boldsymbol{s}\cdot[\boldsymbol{v}] \right) \begin{pmatrix} \mathrm{sym}(\boldsymbol{s}\otimes\boldsymbol{n}) \\ \rho^- c_s^- \boldsymbol{s} \end{pmatrix} \\ &+ \left(\frac{c_s^- c_s^+}{\mu^+ c_s^- + \mu^- c_s^+} \boldsymbol{t}\cdot[\![\boldsymbol{S}]\!] + \frac{c_s^- \mu^+}{\mu^+ c_s^- + \mu^- c_s^+} \boldsymbol{t}\cdot[\boldsymbol{v}] \right) \begin{pmatrix} \mathrm{sym}(\boldsymbol{t}\otimes\boldsymbol{n}) \\ \rho^- c_s^- \boldsymbol{t} \end{pmatrix} = \mathfrak{F}^-\boldsymbol{q}^- + \frac{c_p^- c_p^+ \boldsymbol{n}\cdot[\![\boldsymbol{S}]\!] + c_p^-(\lambda^+ + 2\mu^+)[\![\boldsymbol{v}]\!]}{c_p^+(\lambda^- + 2\mu^-) + c_p^-(\lambda^+ + 2\mu^+)} \begin{pmatrix} \boldsymbol{n}\otimes\boldsymbol{n} \\ \rho^- c_p^- \boldsymbol{n} \end{pmatrix} \\ &- \frac{c_s^- c_s^+}{\mu^+ c_s^- + \mu^- c_s^+} \begin{pmatrix} \mathrm{sym}(\boldsymbol{n}\otimes(\boldsymbol{n}\times(\boldsymbol{n}\times[\![\boldsymbol{S}]\!]))) \\ \rho^- c_s^- \boldsymbol{n}\times(\boldsymbol{n}\times[\![\boldsymbol{S}]\!]) \end{pmatrix} - \frac{c_s^- \mu^+}{\mu^+ c_s^- + \mu^- c_s^+} \begin{pmatrix} \mathrm{sym}(\boldsymbol{n}\otimes(\boldsymbol{n}\times(\boldsymbol{n}\times[\boldsymbol{v}]))) \\ \rho^- c_s^- \boldsymbol{n}\times(\boldsymbol{n}\times[\boldsymbol{v}]) \end{pmatrix},\end{aligned}$$

$$(\mathfrak{F}\boldsymbol{q})^* = \mathfrak{F}^-\boldsymbol{q}^- + \frac{\boldsymbol{n}\cdot[\![\boldsymbol{S}]\!] + \rho^+ c_p^+ [\![\boldsymbol{v}]\!]}{\rho^+ c_p^+ + \rho^- c_p^-} \begin{pmatrix} \boldsymbol{n}\otimes\boldsymbol{n} \\ \rho^- c_p^- \boldsymbol{n} \end{pmatrix} - \frac{1}{\rho^- c_s^-} \begin{pmatrix} \mathrm{sym}(\boldsymbol{n}\otimes(\boldsymbol{n}\times(\boldsymbol{n}\times[\![\boldsymbol{S}]\!]))) \\ \rho^- c_s^- \boldsymbol{n}\times(\boldsymbol{n}\times[\![\boldsymbol{S}]\!]) \end{pmatrix}.$$

- Traditional upwind acoustic-elastic fluxes are complex to derive.
- Cannot prove energy stability in the case of heterogeneous media.

Wilcox, Stadler, Burstedde, Ghattas (2010). *A high-order discontinuous Galerkin method for wave propagation through coupled elastic–acoustic media*.

Energy stable acoustic-elastic coupling (with Guo)

$$\boldsymbol{A}_n = \boldsymbol{A}_1 n_x + \boldsymbol{A}_2 n_y + \boldsymbol{A}_3 n_z \qquad \text{(Elastic)}$$

$$\frac{1}{2}\left(\boldsymbol{A}_n^T(\boldsymbol{\sigma}^+ - \boldsymbol{\sigma}) + \tau_{\boldsymbol{v}} \boldsymbol{A}_n^T \boldsymbol{A}_n (\boldsymbol{v}^+ - \boldsymbol{v})\right)$$

$$\frac{1}{2}\left(\boldsymbol{A}_n(\boldsymbol{v}^+ - \boldsymbol{v}) + \tau_{\boldsymbol{\sigma}} \boldsymbol{A}_n \boldsymbol{A}_n^T(\boldsymbol{\sigma}^+ - \boldsymbol{\sigma}) \cdot \boldsymbol{n}\right) \boldsymbol{n}$$

$$\frac{1}{2}\left((\boldsymbol{u}^+ - \boldsymbol{u}) \cdot \boldsymbol{n} + \tau_p (p^+ - p)\right)$$

$$\frac{1}{2}\left((p^+ - p) + \tau_{\boldsymbol{u}} (\boldsymbol{u}^+ - \boldsymbol{u}) \cdot \boldsymbol{n}\right) \boldsymbol{n}$$

$$\text{(Acoustic)}$$

Energy stable acoustic-elastic coupling (with Guo)

(Elastic)

$$\frac{1}{2}\boldsymbol{A}_n\left(\boldsymbol{n}\boldsymbol{n}^T(\boldsymbol{u}-\boldsymbol{v})+\tau_{\boldsymbol{\sigma}}(p\boldsymbol{n}-\boldsymbol{A}_n^T\boldsymbol{\sigma})\right)$$

$$\frac{1}{2}\boldsymbol{n}^T\left(p\boldsymbol{n}-\boldsymbol{A}_n^T\boldsymbol{\sigma}+\left(\boldsymbol{I}-\boldsymbol{n}\boldsymbol{n}^T\right)\boldsymbol{A}_n^T\boldsymbol{\sigma}+\tau_{\boldsymbol{v}}(\boldsymbol{u}-\boldsymbol{v})\right)$$

$$\boldsymbol{u}\cdot\boldsymbol{n}=\boldsymbol{v}\cdot\boldsymbol{n}$$
$$\boldsymbol{A}_n^T\boldsymbol{\sigma}=p\boldsymbol{n}$$

$$\frac{1}{2}\boldsymbol{n}^T\left(\boldsymbol{v}-\boldsymbol{u}+\tau_p(\boldsymbol{A}_n^T\boldsymbol{\sigma}-p\boldsymbol{n})\right)$$

$$\frac{1}{2}\boldsymbol{n}\boldsymbol{n}^T\left(\boldsymbol{A}_n^T\boldsymbol{\sigma}-p\boldsymbol{n}+\tau_{\boldsymbol{u}}(\boldsymbol{v}-\boldsymbol{u})\right)$$

(Acoustic)

Numerical results: coupled acoustic-elastic media

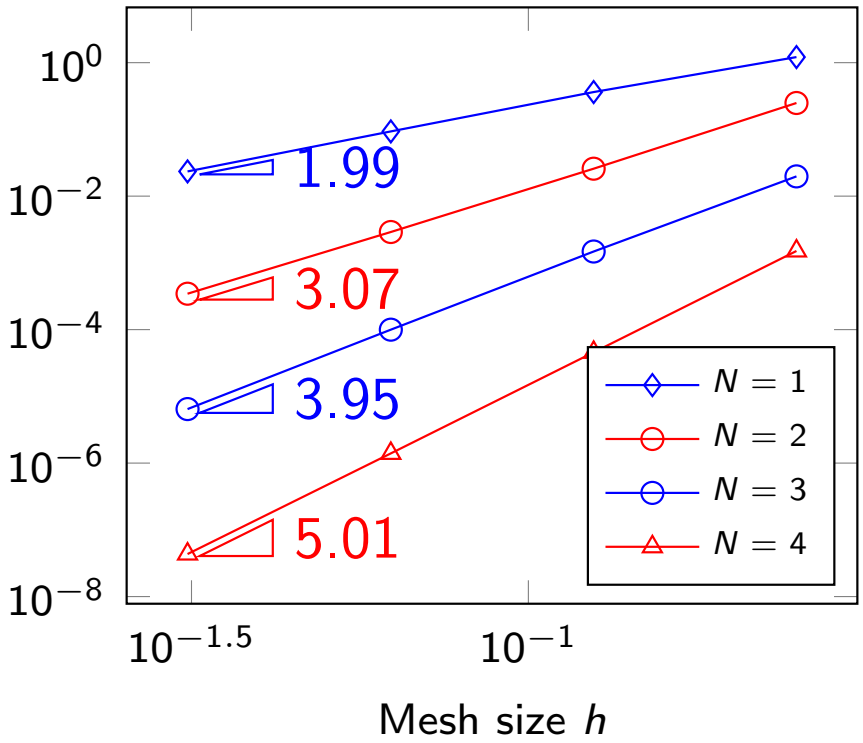

(a) Snell's law solution

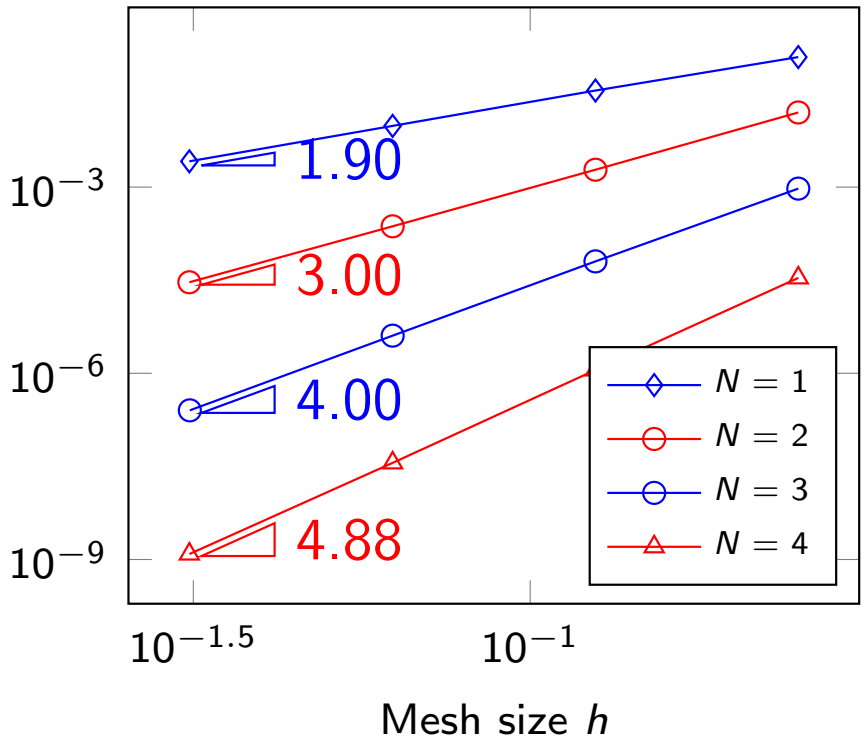

(b) Scholte wave solution

High order convergence of L^2 error for acoustic-elastic media.

Example with isotropic-anisotropic acoustic-elastic media

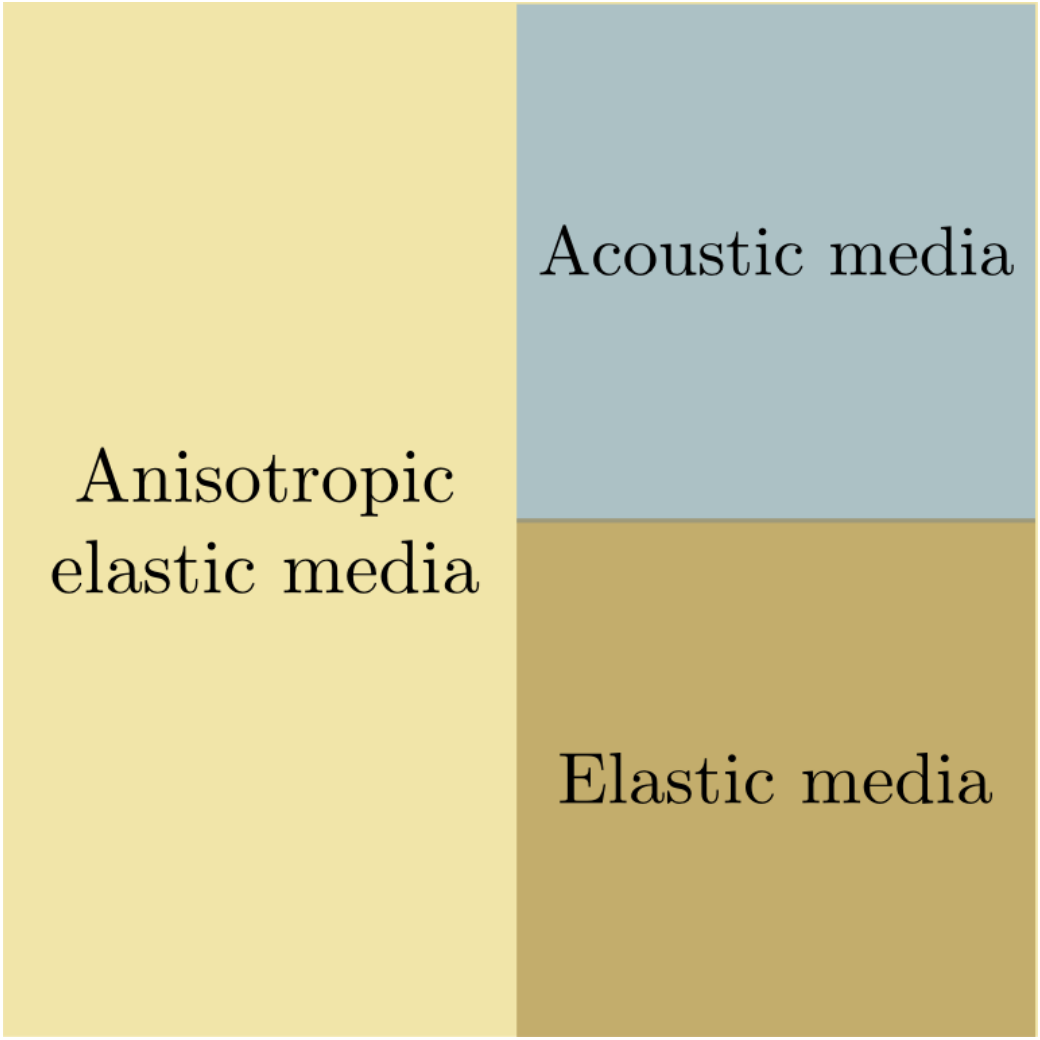

Komatitsch, Barnes, Tromp (2000). *Simulation of anisotropic wave propagation based upon a spectral element method.*

Guo, Acosta, Chan (2019). A weight-adjusted DG method for wave propagation in coupled elastic-acoustic media.

Example with isotropic-anisotropic acoustic-elastic media

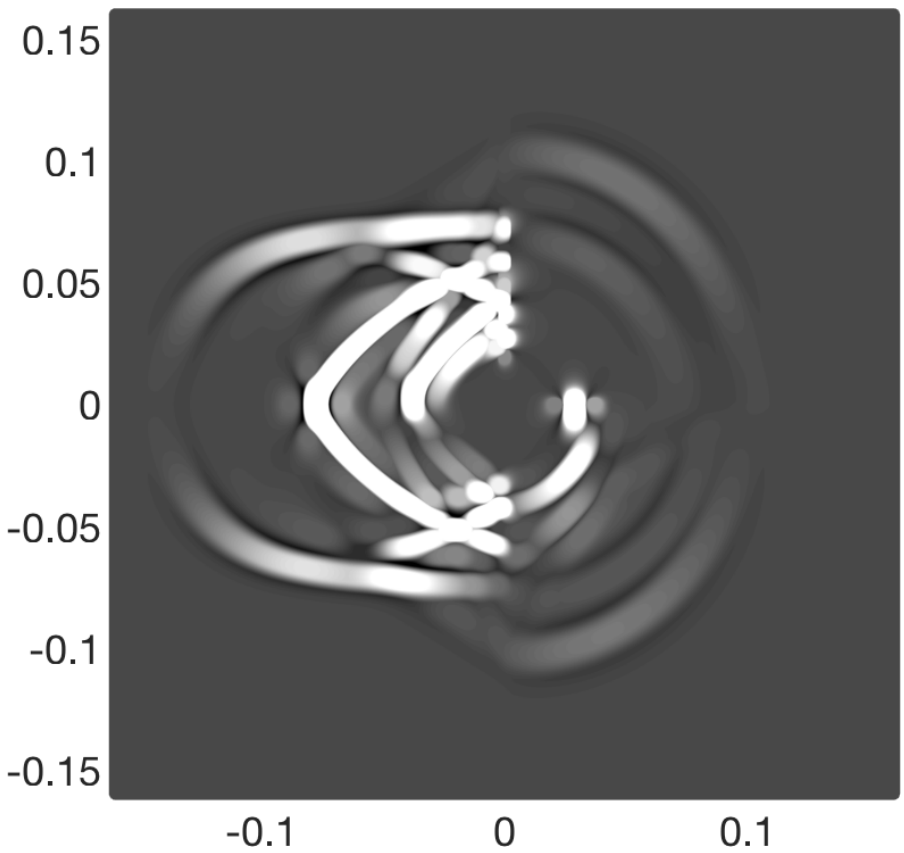

(a) $T = 30\mu s$

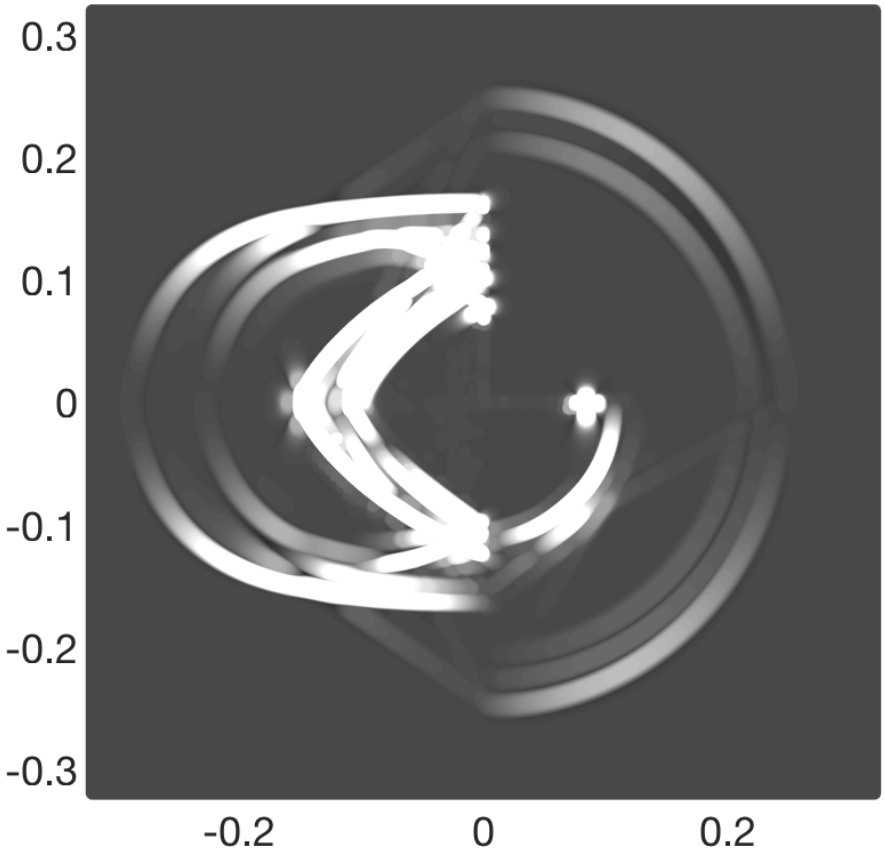

(b) $T = 60\mu s$

Piecewise constant anisotropic-isotropic acoustic-elastic media.

Komatitsch, Barnes, Tromp (2000). *Simulation of anisotropic wave propagation based upon a spectral element method.*

Guo, Acosta, Chan (2019). A weight-adjusted DG method for wave propagation in coupled elastic-acoustic media.

Example with isotropic-anisotropic acoustic-elastic media

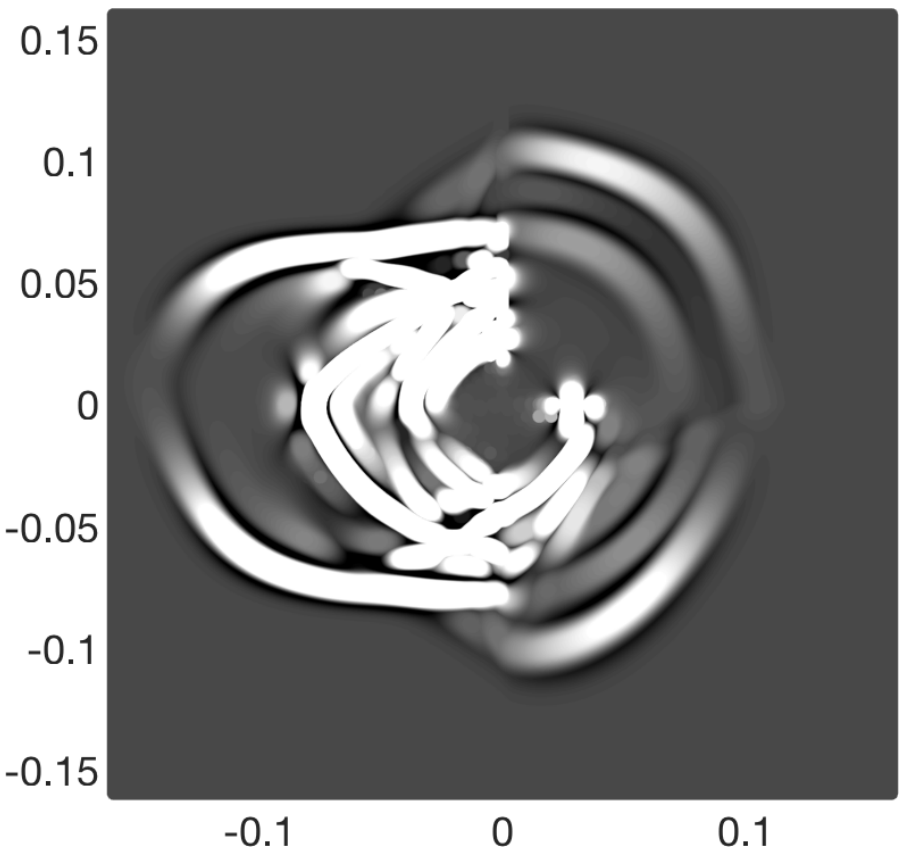

(a) $T = 30\mu s$

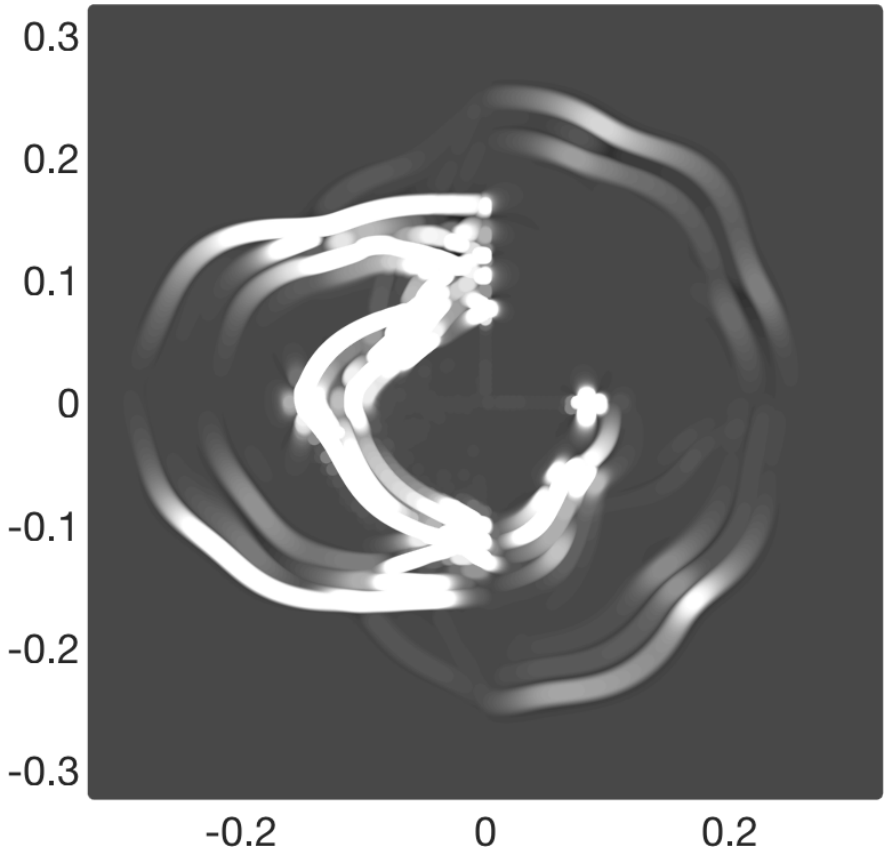

(b) $T = 60\mu s$

Piecewise smoothly varying anisotropic-isotropic acoustic-elastic media.

Komatitsch, Barnes, Tromp (2000). *Simulation of anisotropic wave propagation based upon a spectral element method.*

Guo, Acosta, Chan (2019). A weight-adjusted DG method for wave propagation in coupled elastic-acoustic media.

Outline

1 Weight-adjusted DG (WADG) methods
- High order heterogeneous media
- Curvilinear meshes

2 Elastic and coupled acoustic-elastic media

3 Bernstein-Bezier WADG: high order efficiency

Computational costs at high orders of approximation

Problem: WADG at high orders becomes **expensive**!

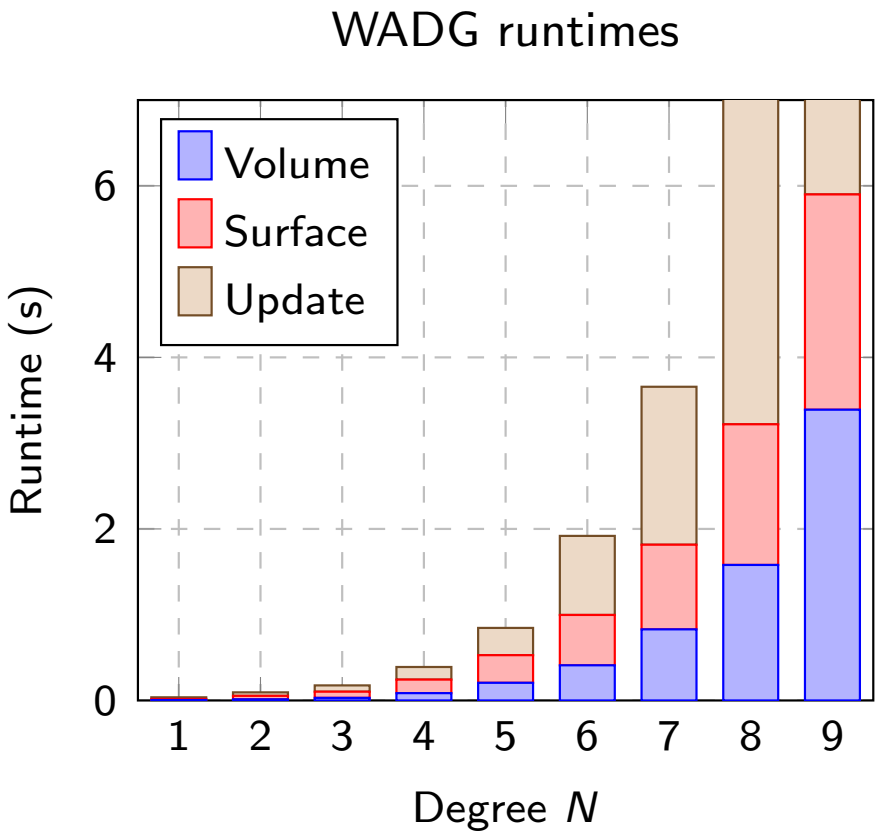

- Large **dense** matrices: $O(N^6)$ work per element.
- Idea: choose basis such that matrices are **sparse**.

WADG runtimes for 50 timesteps, 98304 elements.

BBDG: Bernstein-Bezier DG methods

- Nodal DG: $O(N^6)$ cost in 3D vs $O(N^3)$ degrees of freedom.
- Switch to Bernstein basis: sparse and structured matrices.
- Optimal $O(N^3)$ application of differentiation and lifting matrices.

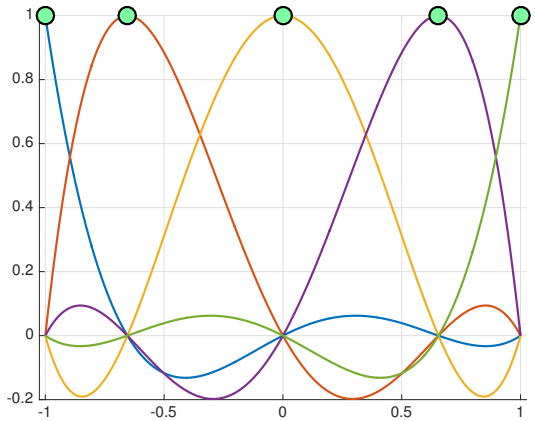

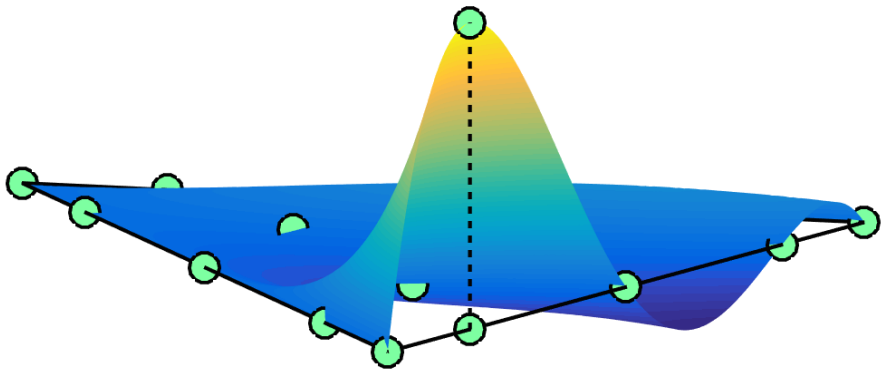

Nodal bases in one, two, and three dimensions.

Chan, Warburton 2017. GPU-accelerated Bernstein-Bezier discontinuous Galerkin methods for wave propagation (SISC).

BBDG: Bernstein-Bezier DG methods

- Nodal DG: $O(N^6)$ cost in 3D vs $O(N^3)$ degrees of freedom.
- Switch to Bernstein basis: sparse and structured matrices.
- Optimal $O(N^3)$ application of differentiation and lifting matrices.

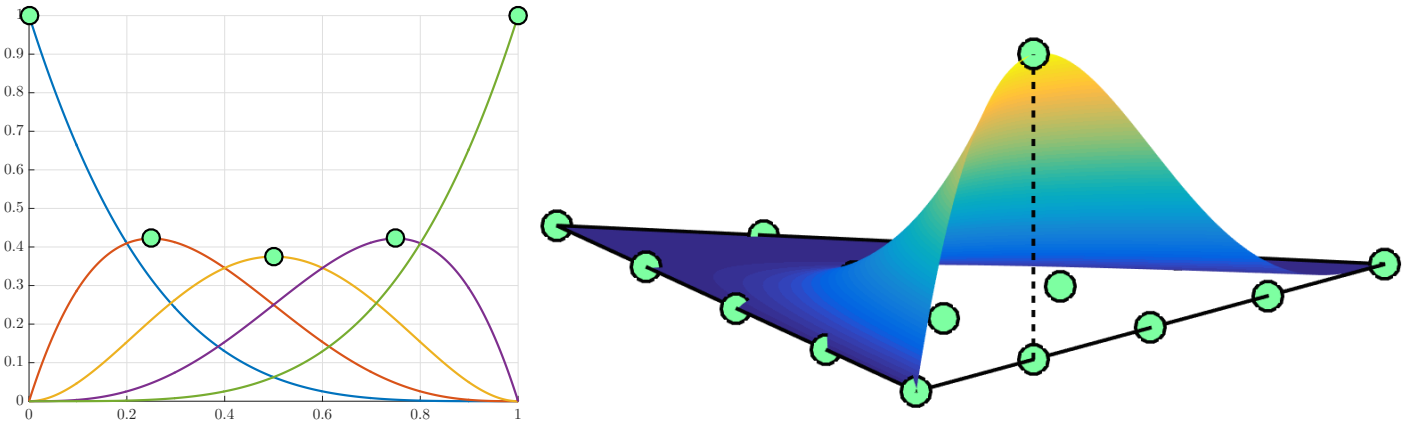

Bernstein bases in one, two, and three dimensions.

Chan, Warburton 2017. GPU-accelerated Bernstein-Bezier discontinuous Galerkin methods for wave propagation (SISC).

BBDG: Bernstein-Bezier DG methods

- Nodal DG: $O(N^6)$ cost in 3D vs $O(N^3)$ degrees of freedom.
- Switch to Bernstein basis: sparse and structured matrices.
- Optimal $O(N^3)$ application of differentiation and lifting matrices.

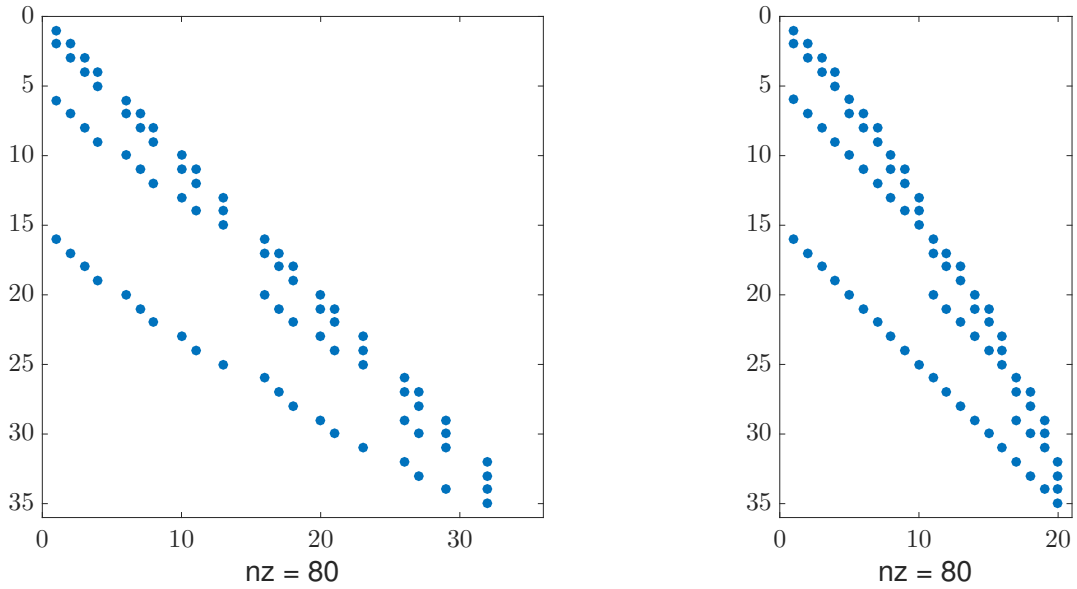

Tetrahedral Bernstein differentiation and degree elevation matrices.

Chan, Warburton 2017. GPU-accelerated Bernstein-Bezier discontinuous Galerkin methods for wave propagation (SISC).

BBDG: Bernstein-Bezier DG methods

- Nodal DG: $O(N^6)$ cost in 3D vs $O(N^3)$ degrees of freedom.
- Switch to Bernstein basis: sparse and structured matrices.
- Optimal $O(N^3)$ application of differentiation and lifting matrices.

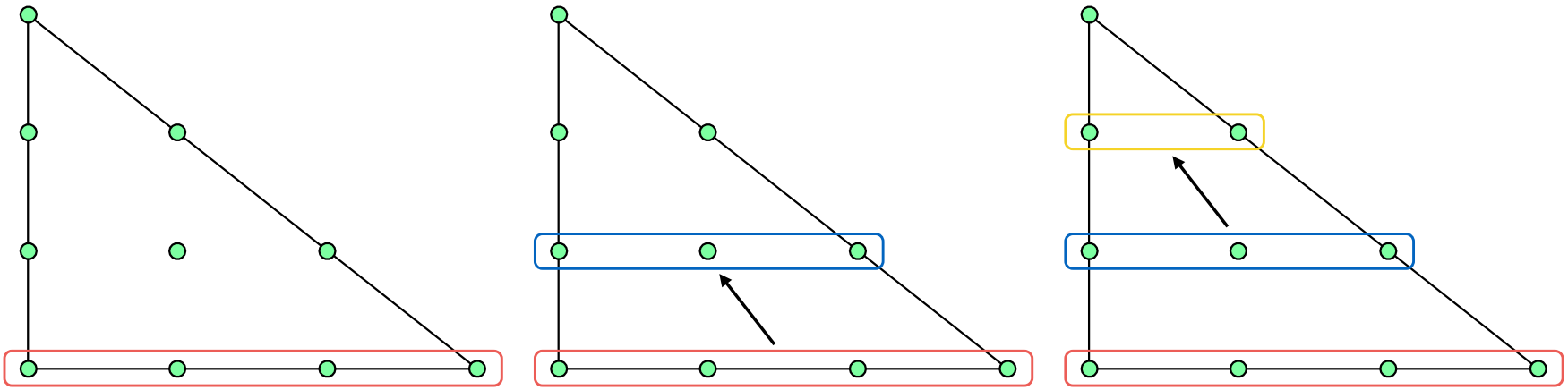

Optimal $O(N^3)$ complexity "slice-by-slice" application of Bernstein lift.

Chan, Warburton 2017. GPU-accelerated Bernstein-Bezier discontinuous Galerkin methods for wave propagation (SISC).

BBDG: efficient volume, surface kernels

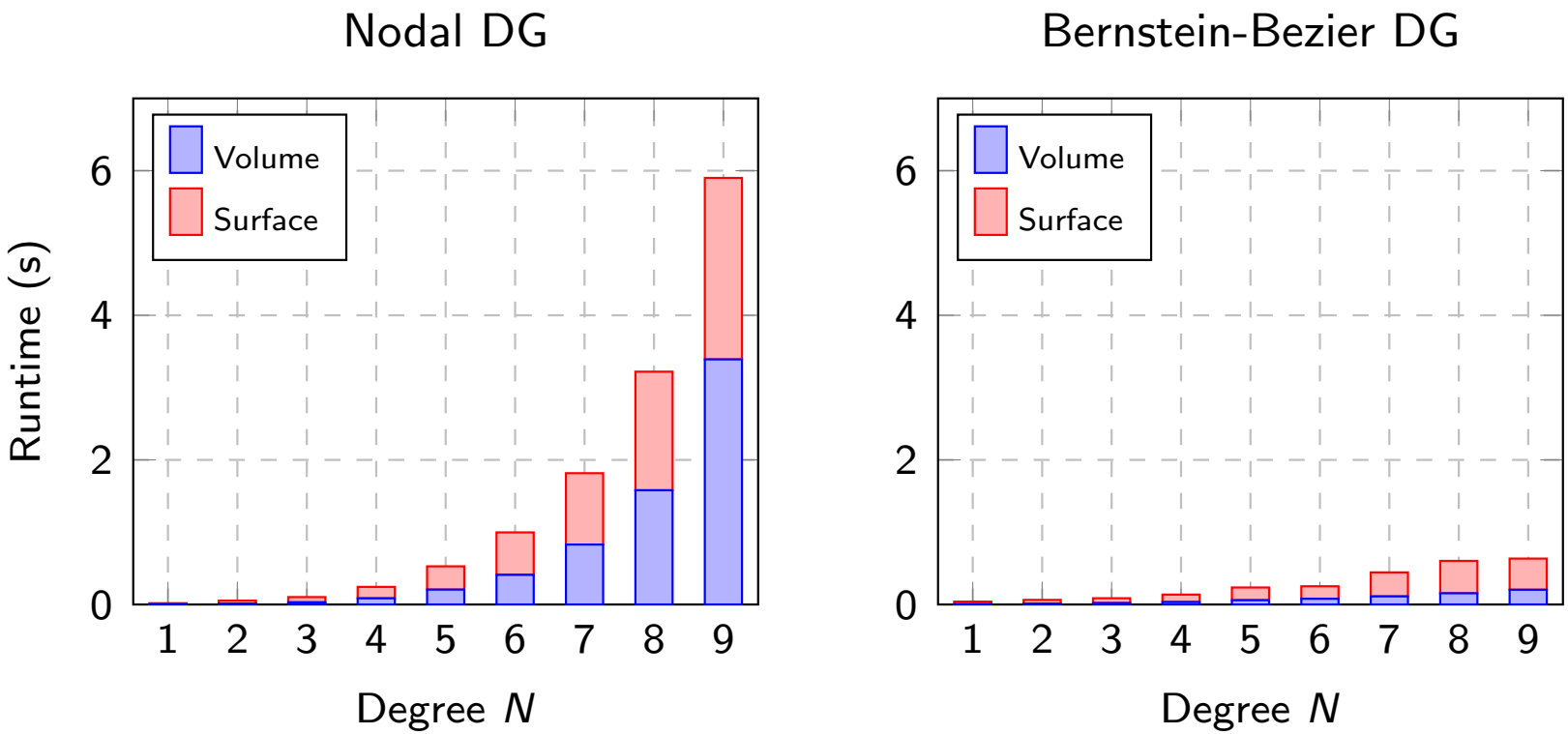

$$\underbrace{\frac{\mathrm{d}\mathbf{u}}{\mathrm{d}t}}_{\text{Update kernel}} = \underbrace{\mathbf{D}_x\mathbf{u}}_{\text{Volume kernel}} + \underbrace{\sum_{\text{faces}} \mathbf{L}_f\,(\text{flux})}_{\text{Surface kernel}}, \quad \mathbf{L}_f = \mathbf{M}^{-1}\mathbf{M}_f.$$

A faster BBWADG update kernel (with Guo)

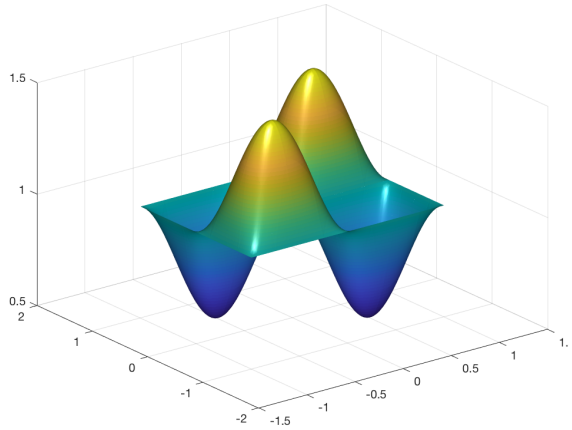

(a) Exact c^2

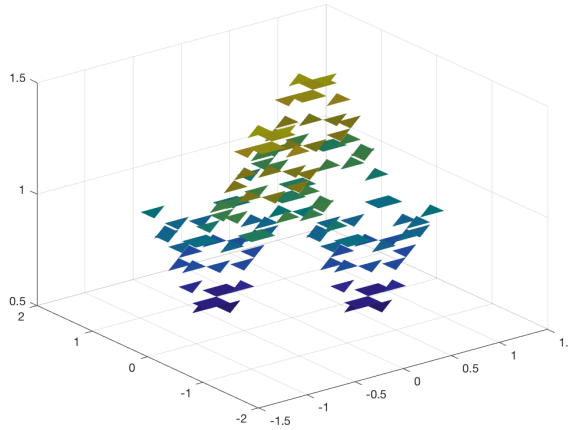

(b) $M = 0$ approximation

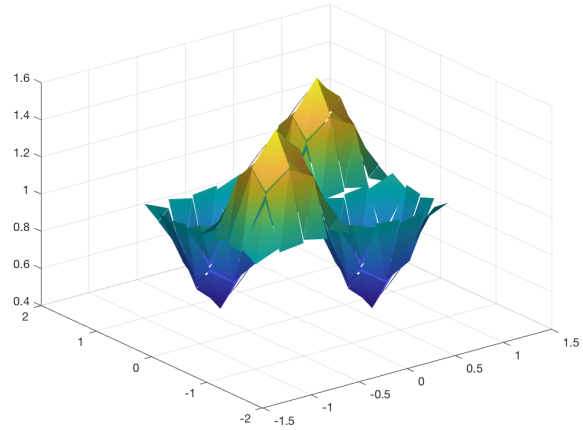

(c) $M = 1$ approximation

- Exploit continuous WADG steps: given $u(\boldsymbol{x})$, compute

$$P_N \left(u(\boldsymbol{x}) c^2(\boldsymbol{x}) \right), \qquad P_N = L^2 \text{ projection operator.}$$

- Our approach: approx. $c^2(\boldsymbol{x})$ with degree M polynomial, use fast Bernstein algorithms for polynomial multiplication and projection.
- Can reuse fast $O(N^3)$ Bernstein-based volume and surface kernels.

BBWADG: effect of approximating c^2 on accuracy

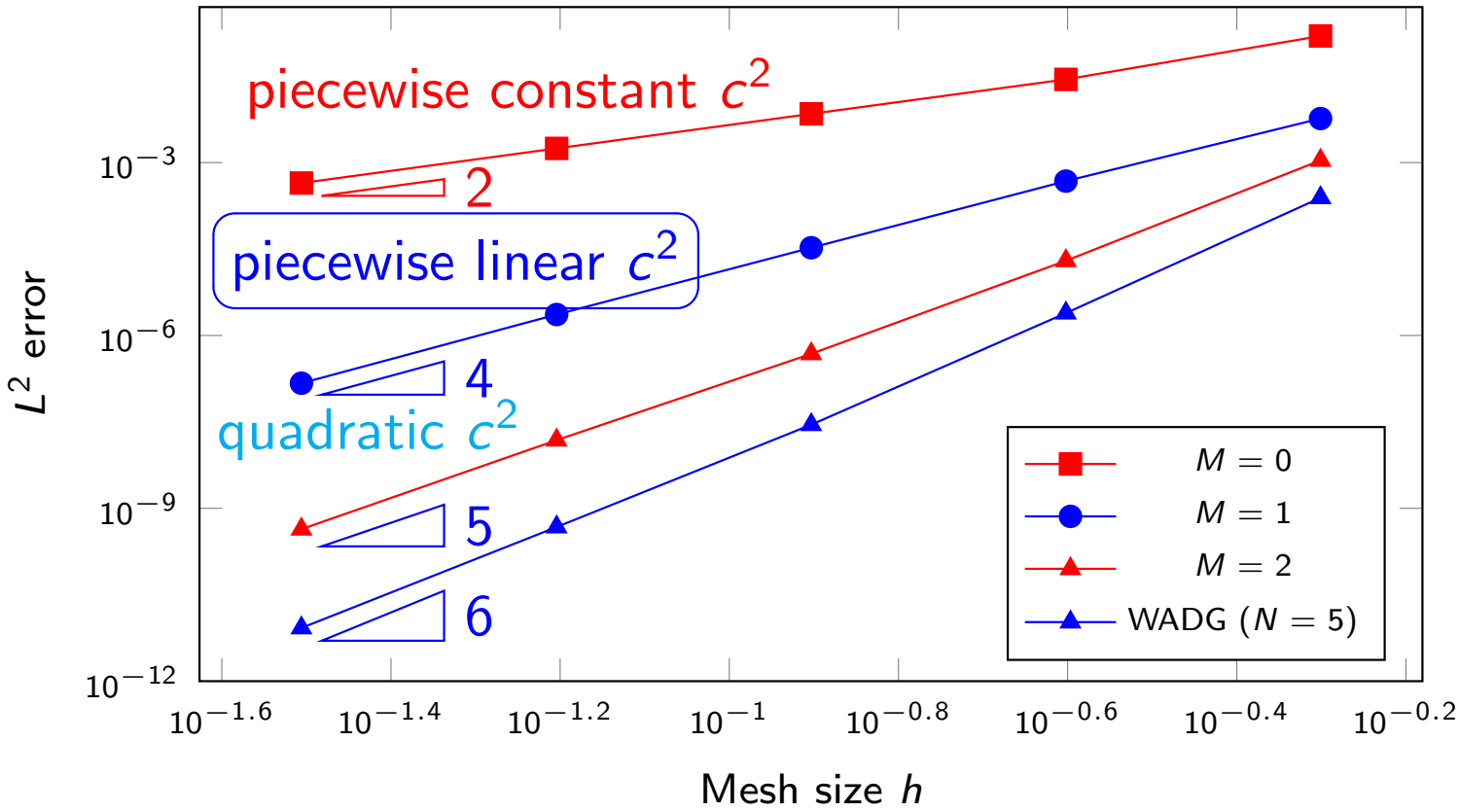

Approximating smooth $c^2(\boldsymbol{x})$ using L^2 projection:
$O(h^2)$ for $M = 0$, $O(h^4)$ for $M = 1$, $O(h^{M+3})$ for $0 < M \leq N - 2$.

Fast Bernstein polynomial multiplication

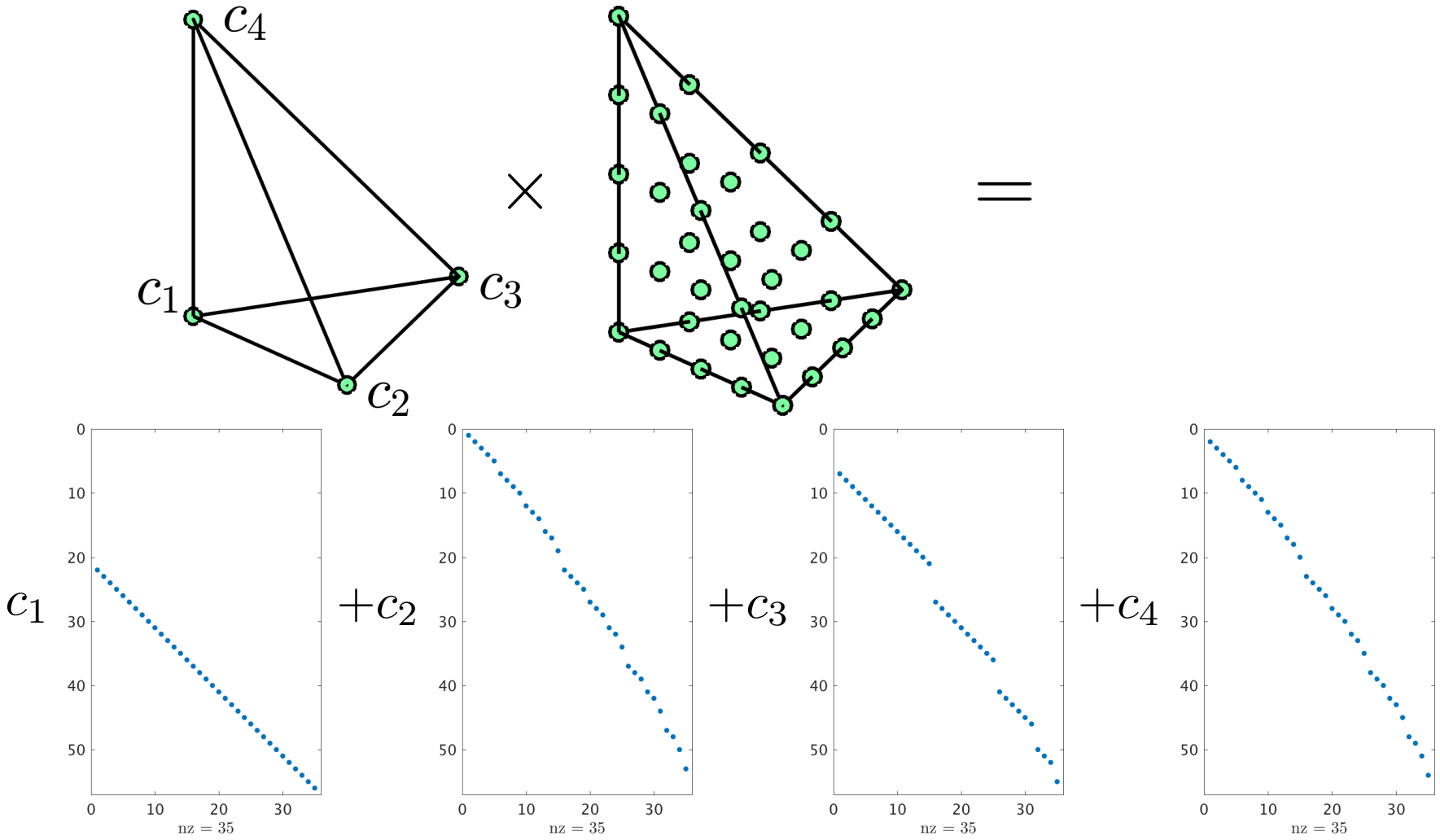

Bernstein polynomial multiplication ($M = 1$ shown), $O(N^3)$ cost for fixed M.

Fast Bernstein polynomial projection

- Given $c^2(\boldsymbol{x})u(\boldsymbol{x})$ as a degree $(N+M)$ polynomial, apply L^2 projection matrix $\boldsymbol{P}_N^{N+M}$ to reduce to degree N.
- Polynomial L^2 projection matrix $\boldsymbol{P}_N^{N+M}$ under Bernstein basis:

$$\boldsymbol{P}_N^{N+M} = \underbrace{\sum_{j=0}^{N} c_j \boldsymbol{E}_{N-j}^N \left(\boldsymbol{E}_{N-j}^N\right)^T}_{\tilde{\boldsymbol{P}}_N} \left(\boldsymbol{E}_N^{N+M}\right)^T$$

- "Telescoping" form of $\tilde{\boldsymbol{P}}_N$: $O(N^4)$ complexity, more GPU-friendly.

$$\left(c_0 \boldsymbol{I} + \boldsymbol{E}_{N-1}^N \left(c_1 \boldsymbol{I} + \boldsymbol{E}_{N-2}^{N-1} \left(c_2 \boldsymbol{I} + \cdots\right) \left(\boldsymbol{E}_{N-2}^{N-1}\right)^T\right) \left(\boldsymbol{E}_{N-1}^N\right)^T\right)$$

Sketch of GPU algorithm for $\tilde{P}_N$

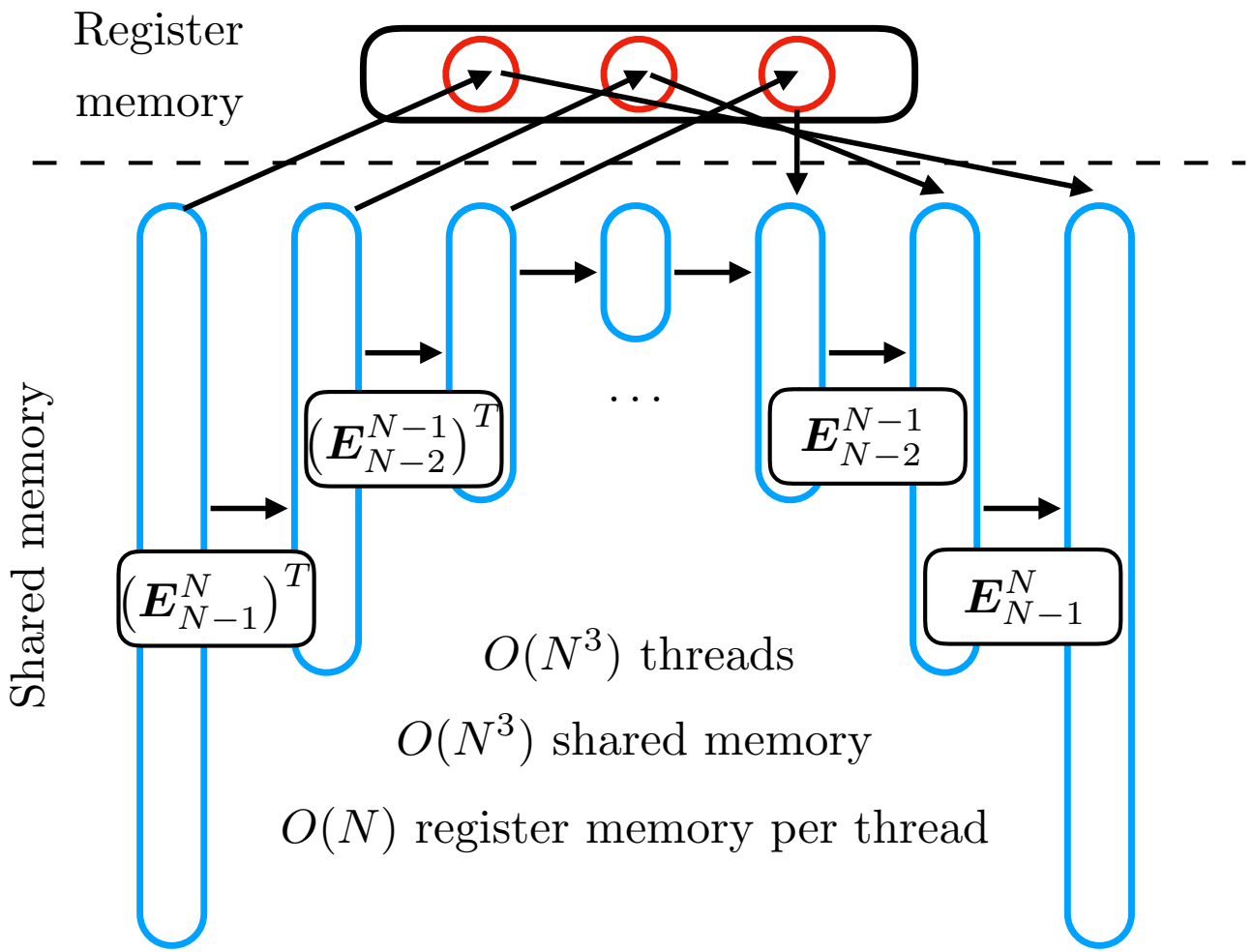

$$\left(c_0\boldsymbol{I}+\boldsymbol{E}_{N-1}^{N}\left(c_1\boldsymbol{I}+\boldsymbol{E}_{N-2}^{N-1}\left(c_2\boldsymbol{I}+\cdots\right)\left(\boldsymbol{E}_{N-2}^{N-1}\right)^T\right)\left(\boldsymbol{E}_{N-1}^{N}\right)^T\right)$$

BBWADG: computational runtime (3D acoustics)

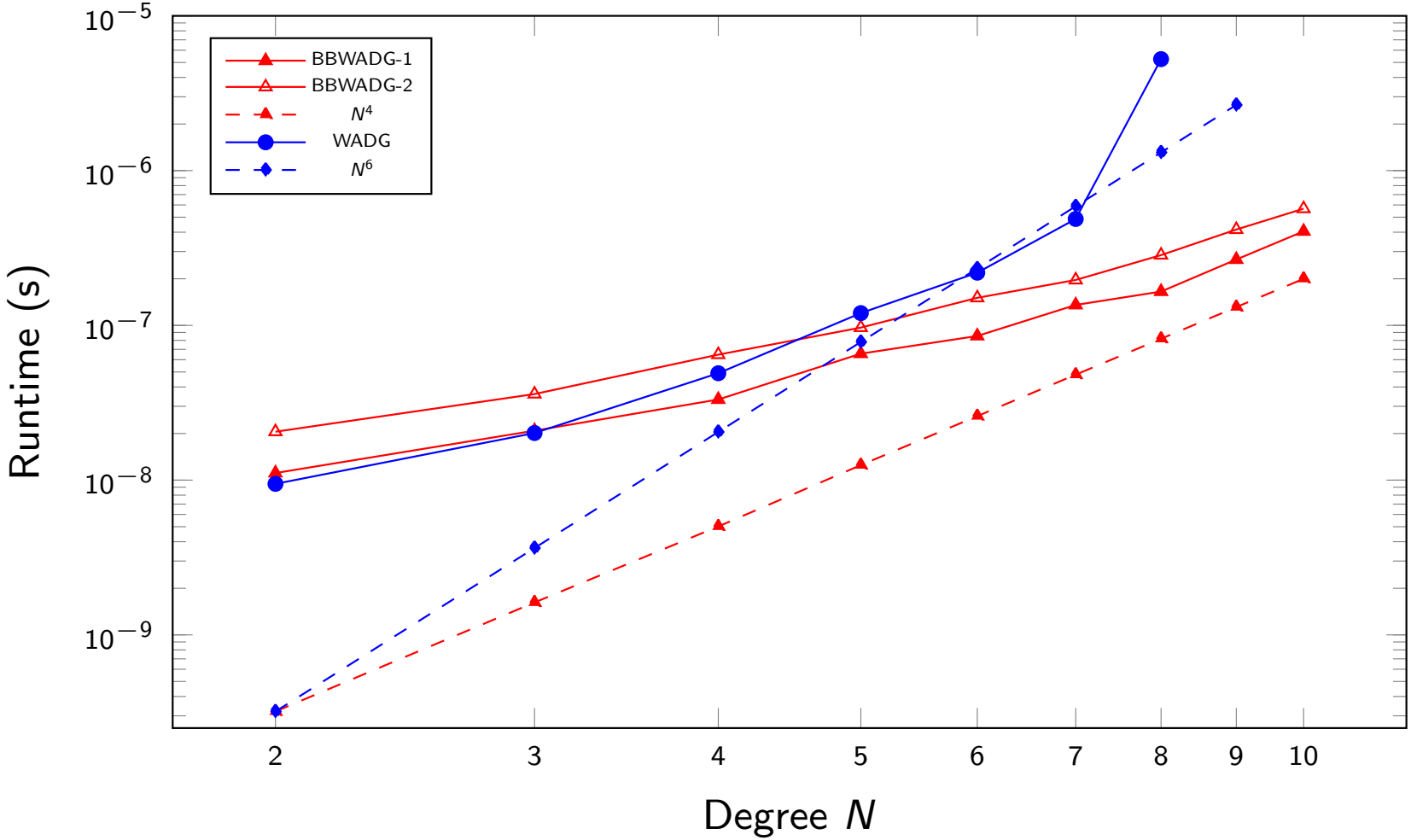

Per-element runtimes of update kernels for BBWADG vs WADG (acoustic). We observe an asymptotic complexity of $O(N^4)$ per element for $N \gg 1$.

Summary and acknowledgements

- Weight-adjusted DG: high order accuracy, provable stability, and efficiency for complex heterogeneous media and curved meshes.
- BBWADG: improved efficiency at high orders of approximation.
- This work is supported by NSF DMS-1712639 and DMS-1719818.

Thank you! Questions?

Guo, Chan (2020). Bernstein-Bézier weight-adjusted DG methods for wave propagation in heterogeneous media.

Guo, Acosta, Chan (2019). A weight-adjusted DG method for wave propagation in coupled elastic-acoustic media.

Chan, Evans (2018). Multi-patch DG-IGA for wave propagation: explicit time-stepping and efficient mass matrix inversion.

Chan (2018). Weight-adjusted DG methods: matrix-valued weights and elastic wave prop. in heterogeneous media.

Chan, Hewett, Warburton (2017). Weight-adjusted DG methods: curvilinear meshes.

Chan, Hewett, Warburton (2017). Weight-adjusted DG methods: wave propagation in heterogeneous media.

Chan, Warburton (2017). GPU-accelerated Bernstein-Bezier discontinuous Galerkin methods for wave propagation.

Additional slides

Existing approaches: mass lumping

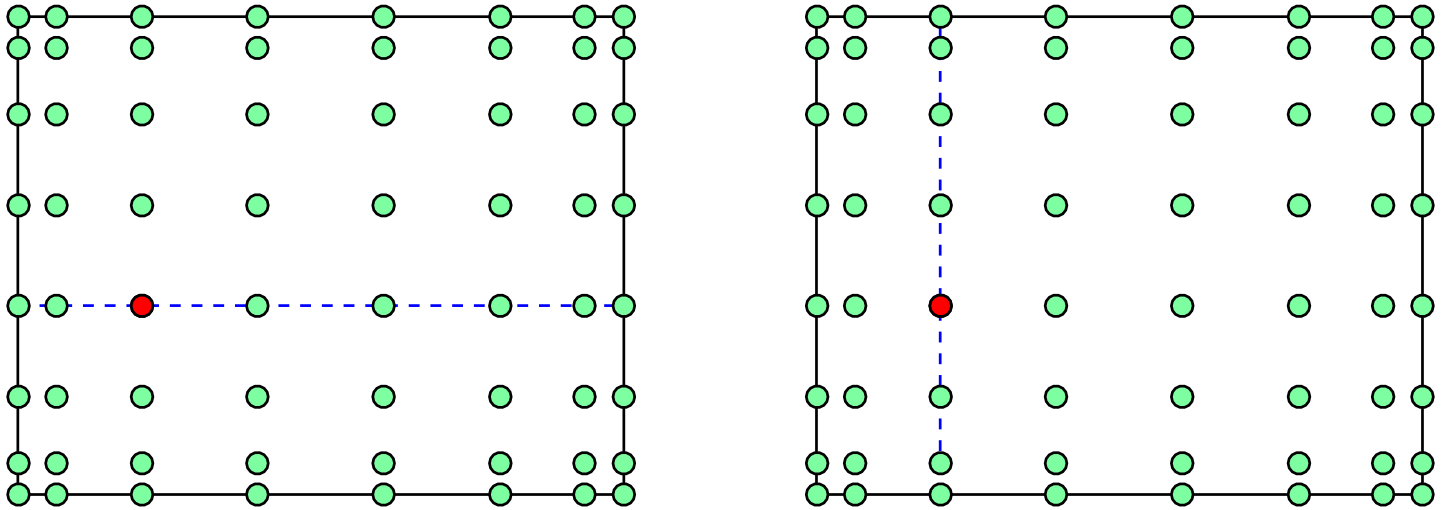

- DG-SEM: collocate at Gauss-Lobatto (or Gauss) points for a diagonal mass matrix. $O(N^4)$ total cost in 3D using Kronecker product.
- Limited to polynomial quads/hexes! Loss of stability or accuracy when extending to simplices (or prisms, pyramids, or non-polynomials).

Chan, Evans (2018). Multi-patch DG-IGA for wave propagation: explicit time-stepping and efficient mass matrix inversion.

Banks, Hagstrom (2016). On Galerkin difference methods.

BBWADG: computational runtime (3D elasticity)

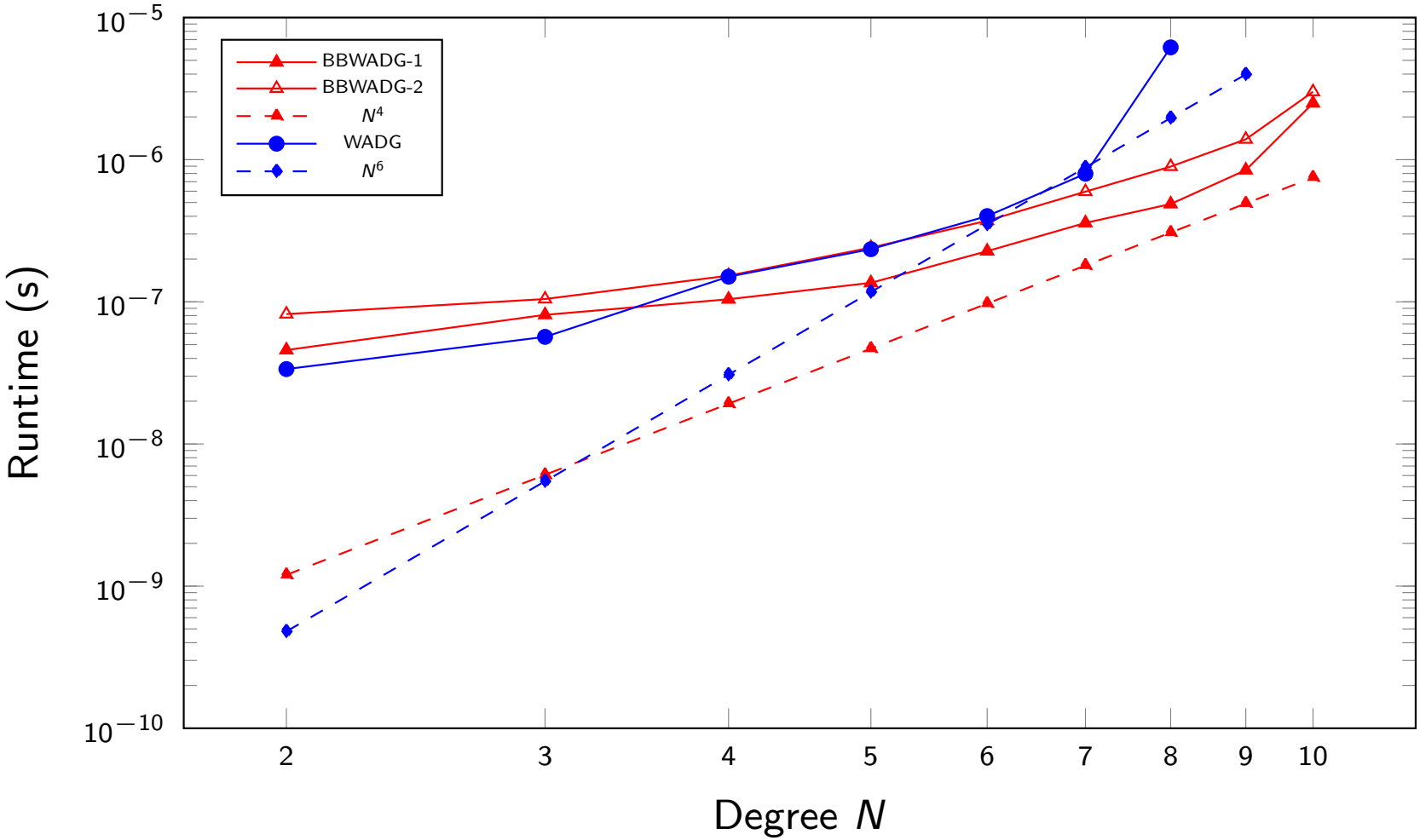

Per-element runtimes of update kernels for BBWADG vs WADG (elastic). For N large, heavy use of register memory results in some loss in performance.

BBWADG: update kernel speedup (3D acoustics)

	$N = 3$	$N = 4$	$N = 5$	$N = 6$	$N = 7$
WADG	1.65e-8	3.35e-8	6.94e-8	1.31e-7	3.28e-7
BBWADG	1.81e-8	2.59e-8	4.22e-8	6.16e-8	9.79e-8
Speedup	0.9116	1.2934	1.6445	2.1266	3.3504

Table: Achieved speedup for $M = 1$

	$N = 3$	$N = 4$	$N = 5$	$N = 6$	$N = 7$
WADG	2.02e-8	4.91e-8	1.20e-7	2.19e-7	4.87e-7
BBWADG	3.60e-8	6.47e-8	9.67e-8	1.51e-7	1.97e-7
Speedup	0.5611	0.7589	1.2409	1.4503	2.4721

Table: Achieved speedup for $M = 2$